OTTO-VON-GUERICKE UNIVERSITY, MAGDEBURG
FACULTY OF PROCESS AND SYSTEMS ENGINEERING

Master Thesis

Investigation of the Kinetics of Disintegration Processes during TiO_2 Nanoparticles Synthesis

A thesis submitted in partial fulfillment of the requirements for the award of the degree of

Master of Science in Quality, Safety and Environment

By

Olukayode Isaiah Imole

Magdeburg, Germany; January 2010.

OTTO-VON-GUERICKE-UNIVERSITÄT MAGDEBURG

Fakultät für Verfahrens- und Systemtechnik
Institut für Verfahrenstechnik
Lehrstuhl für Mechanische Verfahrenstechnik
Prof. Dr.-Ing. habil. J. Tomas

Task for Master thesis:

Topic:

Investigation of the kinetics of disintegration processes during TiO_2 nanoparticles synthesis

The design of the nanoparticles for many industrial applications is one of the attractive scientific areas. It is known that Titanium (IV)-oxide has gained much attention in the last few years due to the opportunity e.g. to apply it as a cheap, environmental friendly and nontoxic photocatalyst. The nanoparticles are the most active Titanium (IV)-oxide form due to their high specific surface area and porosity. For the above mentioned application the industrial amount of nanoparticles should be produced. However, one problem remains – to avoid agglomeration and deactivation of the particles. Recently, many studies confirmed that the agglomeration of the particles can be controlled and the agglomerates can be redispersed. Especially, the kinetics of the agglomeration and redispersion processes is important. Many mathematical models are supposed to describe both processes as a tool to control the synthesis of Titanium (IV)-oxide nanoparticles as scale up process. Simultaneously, the control of the agglomeration and redispersion process should be supported by mathematical models. This should be performed by following tasks:

Part A Literature research

The sol-gel process to produce Titanium (IV)-oxide nanoparticles and their stabilization in the suspension against agglomeration should be described. (electrostatic and steric stabilization). The review of relevant literature should include the most popular methods applied for the synthesis of nanoparticles as well as the important parameters that play a role for the morphology and particle size. (heating, stirring rate, disintegration time, presence of stabilizing agent etc.).

Part B Preparation and characterisation of TiO_2 nanoparticles

(1) Preparation of the TiO_2 suspension

The TiO_2 sol has to be prepared under mixing of titanium tertaisopropoxide [Ti $(OC_3H_7)_4$] as a precursor and inorganic acid (nitric acid etc) as solvent. The suspension has to be prepared in different volume ratios and stirred with different stirring rates at 50°C until sol homogenization is achieved. During the up-scaling process, the following parameters should be taken into account.

a. the stirring rate
b. the stirrer geometry
c. the homogenization time

(2) Characterisation of the disintegration process

Particles size distributions have to be measured by photon correlation spectroscopy in order to detect experimentally the agglomeration and redispersion kinetics.

(3) Modelling the kinetics of the agglomeration and disintegration process

In order to illustrate the agglomeration and redispersion processes for the Titanium (IV)-oxide nanoparticles in suspension, an appropriate mathematical model has to be applied. The results should be compared with it.

(4) Isolation of the TiO_2 nanoparticles from suspension by means of centrifugation

The TiO_2 nanoparticles have to be isolated via tube centrifuge with very high centrifugal speed. The morphology of the particles has to be visualised by means of scanning electron microscopy and transmission electron microscopy. The specific surface area of the nanoparticles will be determined via BET-Method.

Beginning of the work: 01.07.2009

Delivery of the work: 31.01.2010

Supervisors of the master thesis: Dr. rer. nat. Werner Hintz

Dipl.-Ing. Veselina Yordanova

Prof. Dr.-Ing. habil. Jürgen Tomas

ACKNOWLEDGMENTS

I am grateful to God for the privilege of studying in Germany. I also appreciate the funding provided by the DAAD scholarship in support of my studies.

I am also indebted to all my family for their love and concern. I am grateful to all my friends at the church in Leipzig, Germany for their spiritual support.

I wish to thank Rajesh Kumar, Bolaji Adesokan and Vincent of the Faculty of Mathematics, Institute of Numerics, Otto-von-Guericke University for their support in the numerical part of this work.

Also, I wish to thank Prof. Dr.-Ing. habil. Jürgen Tomas for the opportunity to work under his supervision. I also appreciate Dr. rer. nat. Werner Hintz for his assistance. I am most indebted to Dipl.-Ing. Veselina Yordanova and Daniel Binev for their support throughout the course of this research. Without these people, this work would have been difficult to accomplish.

TABLE OF CONTENTS

List of figures

Nomenclatures

Alphanumeric Symbols

A	Hamaker constant
a	Particle surface to surface distance
C(x)	ion number concentration
C_0	number concentration
d_F	fractal dimension
Δd_i	width of the ith interval
e	unit electric charge
$f(\kappa a)$	Henry's function.
ΔG	Gibbs free energy
h	Distance between the particle centers
h_i	height of the i_{th} interval
ΔH	enthalpy change
kT	Thermal Energy
k	Boltzmann constant
k_{ip}	agglomeration
l	largest diameter of irregular agglomerates
m	mass of particles formed
n(x)	ion concentration in the vicinity of the charged surface
n_i	number of particles in each interval
N	total number of particles
N	bulk concentration
$Q_r(d)$	cumulative distribution function
$q_r(d)$	particle size frequency distribution
r_i, r_j	particle radius
R	particle center – center distance
s	separation distance between surface of the particles.
S_n	breakage or redispersion rate of aggregates of size p
ΔS	entropy change.

T	temperature
$u(x)$	electric potential at x
$V_t(R)$	total interaction energy,
$V_a(R)$	attraction interaction energy
$V_r(R)$	electrostatic repulsive energy.
x	distance from the surface
z	ion valence
z	zeta potential

Greek Symbols

Ψ	electric potential,
ρ	volume charge density
ε	dielectric constant of the medium.
ψ_0	potential at the surface
ε_0	Dielectric permittivity of the free space
ε_r	Relative permittivity of solvent
η	viscosity
$\propto$	collision efficiency
β_{ij}	collision frequency for particles of volumes i and j
$\gamma_{n,j}$	breakage distribution function defining the volume fraction of the fragments of size n originating from the j-sized particles.
κ^{-1}	Debye length
ϕ_s	Stern potential
ϕ_i	Helmholtz potential
ϕ_0	Nernst potential
μ_E	electrophoretic mobility
$\dot{\gamma}$	shear rate

Abstract

The kinetics of the disintegration process during Titanium (IV) oxide nanoparticles sol-gel synthesis is presented in this work. The purpose is to investigate the opportunities available and optimum conditions for industrial production of TiO_2 nanoparticles, influence of process conditions on the kinetics and how to control and predict the agglomeration and redispersion mechanisms. The TiO_2 sol is prepared by mixing titanium tetraisopropoxide [Ti $(OC_3H_7)_4$] as a precursor and an inorganic acid (nitric acid) as solvent. The suspension was prepared using different volume ratios, stirring rates and stirrer geometries at 50^0C until sol homogenization is achieved. Particle size is measured by photon correlation spectroscopy and isolation of TiO_2 nanoparticles was achieved by freeze drying. Visualisation of particle morphology was by transmission electron microscopy while the specific surface area is determined by via the BET-method. A numerical model based on the cell average technique was employed to simulate the evolution of the particle size distribution thereby validating experimental results by the resolution of population balance equations. The disintegration kernels proposed by Austin and Diemer have also been employed to describe the kinetics of disintegration. Results show that redispersion is the dominant mechanism and the homogenization time is constant regardless of volume ratios of precursor and dispersants, stirrer geometries and stirrer speeds. The effects of these parameters on the dynamic evolution of particle size distributions are minor as experimental and simulation results are comparable. TEM visualizations also confirmed the crystalline nature of Titanium (IV)-oxide nanoparticles while the electrophoretic mobility values obtained confirm the stability of the nanoparticles. This suggests an extensive opportunity for achieving reproducible results for the industrial production of TiO_2 nanoparticles as evidenced from the scale-up experiments performed using optimum process conditions.

CHAPTER 1

INTRODUCTION

1.1 Nanotechnology and Nanoparticles – Overview

Nanotechnology refers to the study of functional materials and systems through control of matter on the atomic scale (1-100 nanometers). This results in the creation of particles with new properties which have one or more dimensions within a critical range of 1 – 100nm. These particles are called Nanoparticles.

Studies on nanoparticles have attracted a lot of scientific interest over the last decade. This has resulted in a significant increase in the body of literature published in this field and scientific findings that suggest that particles engineered on the nanoscale have superior properties when compared with conventional engineering materials. The potential benefits cut across various sectors and include applications for industrial, biological, medical and environmental uses among others. These benefits include:

1. Nanoparticles provide a strong potential for improvements in product performance and the reduction of manufacturing cost.
2. The significant increase in surface area to volume ratio of nanoparticles opens up new possibilities in surface-based science such as their applications as catalysts.
3. Materials engineered in the nanoscale can exhibit properties different from what they show on the macroscale level. For example, Insulators (e.g. silicon) on the macroscale can become conductors on the nanoscale. This opens a new window of exploring these novel properties for further applications.

1.2 Objectives of the Study

Titanium (IV)-oxide nanoparticles have been widely applied in several industrial processes. Photocatalyst TiO_2 has been extensively used for environmental applications because of its high oxidative power, non-toxicity, photostability, and water insolubility properties under most conditions [1-5]. However, its application has been limited due to an inadequate understanding of the kinetics of the agglomeration and redispersion process. We therefore carry out this study in order to achieve the following objectives:

1. To employ sol-gel technique for the synthesis of Titanium (IV) oxide (also called Titanium (IV)-oxide) on the laboratory and investigate the influence of process parameters on the kinetics during the scale-up of the experimental study for insights on the possibilities available for the industrial production of Titanium (IV)-oxide nanoparticles. Such parameters to be investigated would, in general include:
    - The influence of variations in shear rate,
    - The influence of variations in stirrer geometry and
    - The influence of a stepwise increment in the volume of precursor (Titanium tetraisopropoxide) and corresponding increase in dispersant volume while keeping concentration of dispersant (Nitric Oxide) constant at its optimum value (0.1 M).
    - Overall influence of the above parameters on the homogenization time

    Dynamic light scattering will be used in the measurement of particle size distribution and morphology of the nanoparticles will be visualized by transmission electron microscopy.
2. To illustrate the agglomeration and redispersion process by applying an appropriate mathematical models from population balance equations. Experimental and numerical results would thereafter be compared for agreement.
3. To measure the specific surface area of the Titanium (IV)-oxide nanoparticles produced by the BET method and comment on the stability of the nanoparticles by measuring the electrophoretic mobility (zeta potential) of the sol. The particles will be isolated with using freeze drying technique.
4. To draw appropriate conclusions and provide recommendations from the above tasks on the prospects of the industrial production of the Titanium (IV)-oxide nanoparticles

CHAPTER 2

TITANIUM (IV) OXIDE NANOPARTICLES SYNTHESIS IN HOMOGENOUS MEDIUM

The potential of the sol–gel process was not appreciated until 1980, when it was rediscovered and found to be very useful in synthesizing various materials of practical importance. Since then the method has received considerable attention and has been investigated extensively [6]

2.1 Liquid Techniques

Liquid techniques have been used extensively in the preparation of nanoparticles particularly because it provides an opportunity to obtain the desired particle shape and size by controlling the particles during nucleation and growth. Higher efficiencies are thus achieved as the batch process can be operated at low temperatures [7].

2.1.1 Overview of Liquid Techniques

Several techniques have been presented in literature for the preparation of nanoparticles in the liquid medium. It should be noted however that each method presented has its advantages and drawbacks thereby it necessary to understand the technique to be used and the objective to be achieved before they are used. For example, the *hydrothermal process* requires the synthesis of nanoparticles at high temperatures [8]. This results in bigger particles with better crystallographic shape [9]. Also, the *micro-emulsion process* which allows the production of nanoparticles in a nanosized reactor is limited by the difficulty encountered in separating the surfactant from the nanoparticles.

Other techniques available include the chemical precipitation technique [10,11], biomimetric deposition [10], flame spray pyrolysis process [12], solvothermal process [13] and the sol-gel process [10,11].

2.1.2 The Sol-gel Process

The sol-gel process for the preparation of nanoparticles is preferred above other liquid techniques for the following reasons [14]:

- It is possible to derive various special shapes depending on the gel state (e.g. monoliths, films, fibers and monosized powders)
- Low process temperatures make microstructural control possible. This gives the possibility for the development of new materials.
- The precursors used as raw materials for the process are uniform and reproducible.

In the sol-gel process, chemical solutions (typically metal alkoxides or metal chlorides) act as precursors for a complex network of discrete particles or network polymers. These precursors undergo hydrolysis and polycondensation reactions to form metal oxides which can be chemically redispersed to produce nanoparticles.

The production of Titanium (IV) oxide nanoparticles via the sol-gel process is shown below:

Hydrolysis:

$$Ti(OC_3H_7)_4 + 4\ H_2O \longrightarrow Ti(OH)_4 + 4\ C_3H_7OH \qquad (2.1)$$

Polycondensation:

$$Ti(OH)_4 \longrightarrow TiO_2 + 2\ H_2O \qquad (2.2)$$

Redispersion:

$$TiO_2\ (gel) \longrightarrow TiO_2\ (nano) \qquad (2.3)$$

Figure 2.1: Reaction sequence for the sol-gel production of Titanium (IV)-oxide nanoparticles

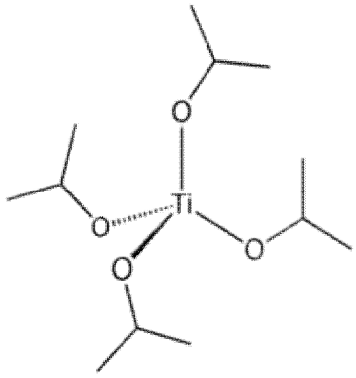

Figure 2.2: The tetrahedral structure of Titanium (IV) isopropoxide molecule

In this reaction, Titanium (IV) isopropoxide (TTIP) is used as the precursor. TTIP is mainly a monomer in nonpolar solvents and is a diamagnetic tetrahedral molecule [10] (see fig. 2.2).

The organic precursor, TTIP reacts with water in an acidic or basic medium and undergoes various forms of hydrolysis and polycondensation reactions to produce large agglomerates of Titanium (IV)-oxide. These agglomerates undergo a slow redispersion reaction to produce Titanium (IV)-oxide nanoparticles.

2.2 Colloidal Stabilization

The major objective of colloidal stabilization is to ensure the stability of the colloids in the liquid medium thereby preventing them from aggregating. Since particles in dispersions are always subjected to Brownian motion, they collide with each other randomly. The interactions (attractive and repulsive) between these particles during collision determine the stability of the colloids. When attraction dominates, the particles adhere to each other and may eventually coalesce. On the other hand, if repulsion dominates, the system will be stable and remain in a dispersed state [16].

The primary forces of attraction between colloidal particles are from Van-der-Waals forces. These forces are always present between particles. Hence, a sufficiently strong repulsive force is necessary to counteract the Van-der-Waals attraction for the dispersion to be stable [16]. Since the London forces – which is one of the origins for Van-der-Waals forces – also contribute to the long-range attraction between colloidal particles, the total magnitude of the Van-der-Waals-London (VDWL) forces must be known in order to determine the measures for stabilizing colloid dispersions.

The various mechanisms available for colloidal stabilization include the following – the electrostatic stabilization, steric stabilization, depletion stabilization and a combination of electrostatic and steric mechanisms known as the electrosteric stabilization.

2.2.1 Electrostatic Stabilization

Electrostatic stabilization involves the use of Coulombic repulsions to counteract the effect of the VDWL forces in colloidal particles. It is known that ionic groups in liquid dispersion media can adsorb to the surface of a colloidal particle through different mechanisms to form a charged layer (an electric potential at the surface). This layer causes a repulsion to exist

between two particles when they approach each other thereby causing them to stick together. It also attracts counter ions to the vicinity of these particles. Since the objective of stabilization is to maintain electro-neutrality, the presence of an equal number of counter-ions with the opposite charge in the solution will surround the colloidal particle and give rise to overall charge-neutral double layers. It is the mutual repulsion of the double layers surrounding the particles that provides stability [17].

2.2.1.1 Electrochemical Double Layer

The double layer theory explains the stability and phase behaviours of colloidal dispersions. It is known that colloidal particles in aqueous suspensions develop a charge at the interface. These charge may arise due to *ionization* (protonation or de-protonation) of surface groups, *ion binding* of solvated ions to globally charge-neutral surfaces that nevertheless contain charge carrying structures, e.g. dipoles in molecules; and by ion exchange where higher valence ions replace lower-valence ions bound to the surface.

In aqueous solution, an ionic atmosphere, or electric double layer develops around charged colloidal particles. If the surface is modelled as an infinitely flat plate, only the radial distance from the surface is relevant. The drop-off of electric potential with distance from the surface is therefore described by the Poisson Equation:

$$\frac{d^2\psi\,(x)}{dx^2} = -\frac{\rho\,(x)}{\varepsilon} \tag{2.4}$$

where ψ is the electric potential, x is the distance from the surface, ρ is the volume charge density at a distance x from the surface, and ε is the dielectric constant of the medium., which is customarily taken to be that of the pure solvent [18]. The volume charge density is always modelled in terms of the Boltzmann distribution. Equation (2.5) gives the Boltzmann expression for ion number concentration in the vicinity of the charged surface, $C(x)$, in terms of the number concentration, C_0, the ion valence, z, the electric potential at x, $\psi(x)$, the unit electric charge, e, and the thermal energy, kT:

$$C(x) = C_0 exp\left(\frac{-ze\Psi(x)}{kT}\right) \tag{2.5}$$

The sum of the Boltzmann factors for all ions present in the solution gives the charge density hence if we combine the two equations above, we obtain the famous Poisson-Boltzmann equation that forms the starting point of the descriptions of the double layer [18].

$$\frac{d^2\psi\,(x)}{dx^2} = -\frac{e}{\varepsilon}\sum_i z_i N_i\, exp\left(\frac{-z_i\, e\psi(x)}{kT}\right) \tag{2.6}$$

The equation shows the ionic atmosphere as an ideal gas of point charges in a dielectric continuum. Hence, the ions in the electrolyte are modelled as point charges of no material dimensions with charge *z*. Thus all monovalent ions are identical in the context of Poisson-Boltzmann theory. If we invoke the Debye- Hückel approximation (assuming a smaller surface potential relative to *kT*), we can express the exponential term as a power series which can be truncated at the linear term to obtain the linearized Poisson – Boltzmann equation:

$$\frac{d^2\psi\,(x)}{dx^2} = \frac{e^2\psi(x)}{\varepsilon kT}\sum_i z^2{}_i N_i \tag{2.7}$$

Combining the physical constants in the equation, we obtain:

$$\kappa^2 = \frac{\sum_i z_i^2 N_i}{\varepsilon kT} \tag{2.8}$$

We can thus express the linearized Poisson-Boltzmann equation as:

$$\frac{d^2\psi\,(x)}{dx^2} = \kappa^2\psi\,(x) \tag{2.9}$$

which gives a solution:

$$\psi\,(x) = \psi_0 \exp(-\kappa x) \tag{2.10}$$

where ψ_0 is the potential at the surface. The Debye-Hückel approximation predicts an exponential decrease in potential with distance from the surface.

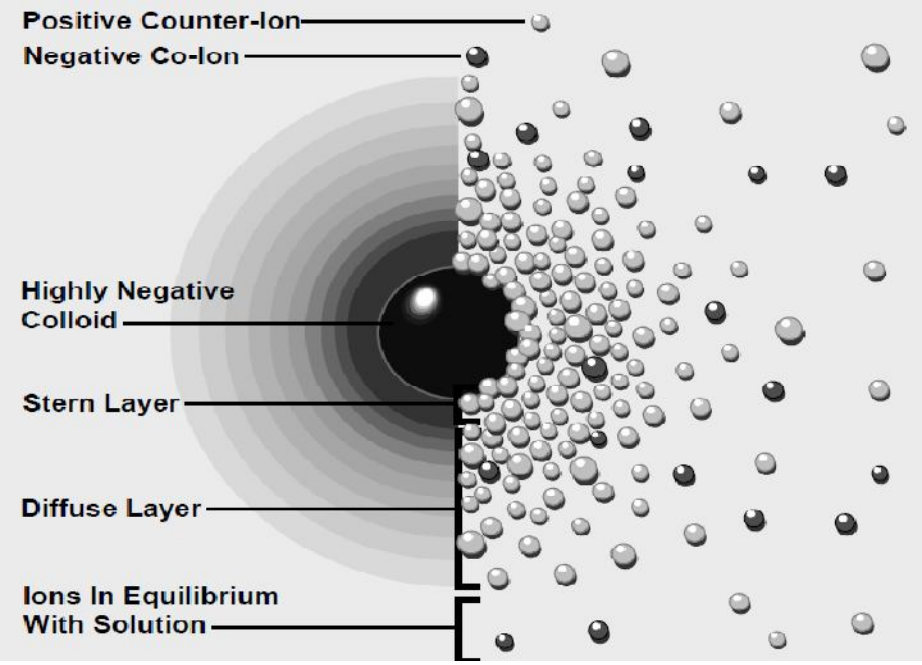

Fig 2.3: A visualization of the Double Layer according to [14].

A visualization of the double layer is depicted in Fig. 2.3 above. The left view shows the change in charge density around the colloid. The right shows the distribution of positive and negative ions around the charged colloid.

2.2.1.2 DLVO Theory

The Derjaguin, Landau, Verwey and Overbeek (DLVO) theory is used as the starting point in understanding the stability and phase behaviours of colloidal dispersions. It describes the total interaction energy between particles as the sum of the attractive and repulsive forces. The DLVO theory depicts the combination of the effects of the van der Waals and double layer (electrostatic repulsion) forces. The theory explains the tendency of colloids to agglomerate by combining the van der Waals attraction curve with the electrostatic repulsion curve to form the net interaction energy curve (see Fig. 2.4). A smaller value is subtracted from the larger at each distance to obtain the net interaction energy curve. The shape of the net curve depends on the dominant mechanism. If there is a repulsive section, the point of maximum repulsive energy is called the energy barrier. This barrier can be altered by varying environmental conditions depending on the objective. By varying the pH or adding surface active materials to directly affect the charge of the colloid, the height of the barrier is adjusted and by

measuring the zeta potential, the impact of the alteration in the stability of the system can be measured.

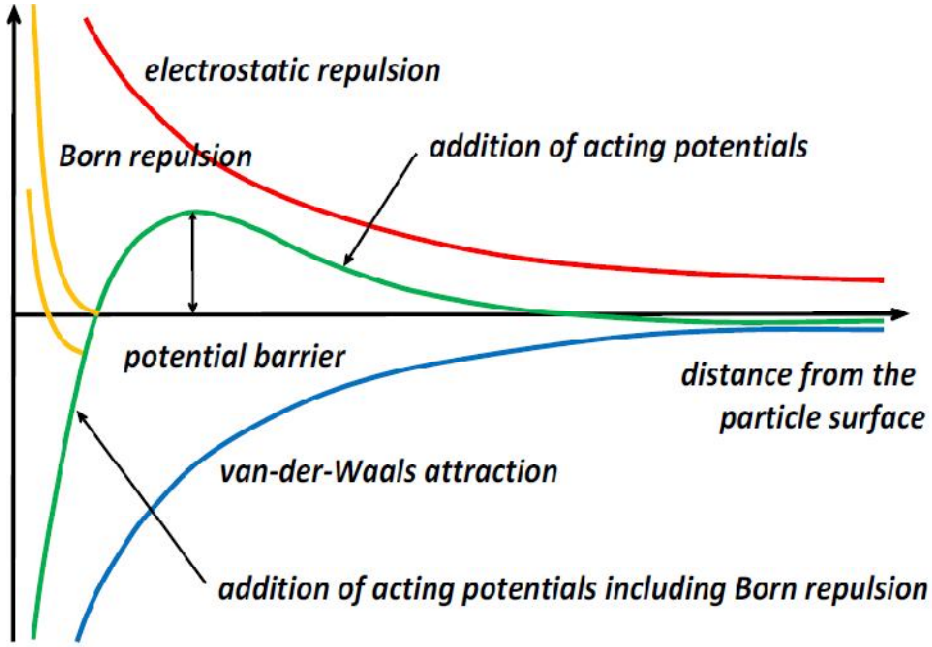

Fig 2.4: Interaction potential between two particles according to the DLVO theory

The height of the energy barrier indicates how stable the system is [19]. For agglomeration to take place, the two particles on collision course must have enough energy (from their velocity and mass) to cross the barrier. Once the barrier is crossed, the net interaction is attractive and agglomeration sets in. The inner region is termed energy trap as the particles trapped in this region are under the influence of the van der Waals forces. Theoretically, we can express the total interaction energy as:

$$V_t(\mathrm{d}) = V_a(d) + V_r(d) \qquad (2.11)$$

where; $V_t(\mathrm{d})$ is the total interaction energy, $V_a(\mathrm{d})$ is attraction interaction energy resulting from van der Waals forces, $V_r(\mathrm{d})$ is the electrostatic repulsive energy and a is the particle surface to surface distance.

We can also express the van der Waals attraction and electrostatic repulsive energy as:

$$V_a(\mathrm{d}) = -\frac{A}{6}\left[\frac{2r_i r_j}{R^2-(r_i+r_j)^2} + \frac{2r_i r_j}{R^2-(r_i-r_j)^2} + ln\left(\frac{R^2-(r_i+r_j)^2}{R^2-(r_i-r_j)^2}\right)\right] \quad (2.12)$$

$$V_r(\mathrm{d}) = 4\pi\varepsilon_r\varepsilon_0\frac{r_i r_j}{R}\psi^2 ln\left[1+\exp\left(-\kappa\left(R-r_i-r_j\right)\right)\right] \quad (2.13)$$

$$A = 12k_bT, \qquad d = R-r_i-r_j \quad (2.14)$$

where;

	A:	Hamaker constant
	ε_0:	Dielectric permittivity of the free space
	ε_r:	Relative permittivity of solvent
	r_i, r_j:	Particle radius
	ψ:	Surface potential of particle
	k:	Boltzmann constant
	R:	Particle center – center distance

2.2.1.3. Zeta Potential

It is known that the formation of the double layer causes an electric potential to exist between the surface of the colloid and any point in the mass of the suspending liquid. This potential is referred to as the surface potential and is in the order of millivolts (mV).

The magnitude of the surface potential is dependent on the surface charge and thickness of the double layer. The potential drops off roughly linearly in the Stern layer and then exponentially through the diffuse layer, approaching a boundary value of 1/e of the surface potential. (see Fig. 2.6) [19].

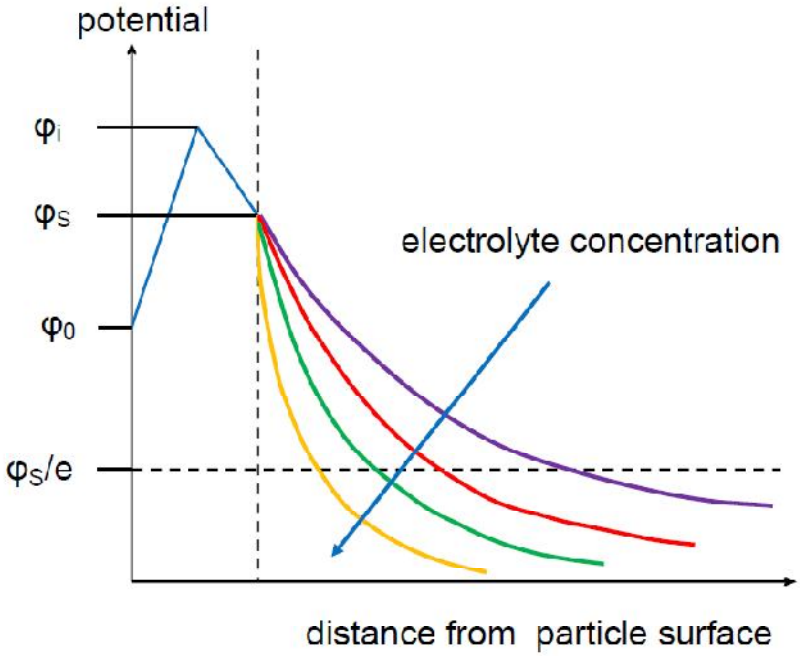

Fig 2.5: Depiction of the relationship zeta potential and surface potential.

Here, ϕ_s is the Stern potential, ϕ_i is the Helmholtz potential and ϕ_0 is the Nernst potential.

An indication of the strength of the electrical force between particles and the corresponding distance at which this force comes into play can be seen from the potential curve. See fig. 2.6 below:

The phenomenon whereby a charged particle moves with a fixed velocity in a voltage field is termed electrophoresis. This mobility is dependent on several factors – the viscosity of the suspending liquid, the dielectric constant and the electric potential at the boundary between the moving particle and the liquid. The boundary (also known as the slip plane) is the point where the stern layer and the diffuse layer meet. The Stern layer is considered to be rigidly attached to the colloid, while the diffuse layer is not. As a result, the electrical potential at this junction is related to the mobility of the particle and is called the zeta potential.

Although zeta potential is an intermediate value, it is sometimes considered to be more significant than surface potential as far as electrostatic repulsion is concerned. Zeta potential can be quantified by tracking the colloidal particles through a microscope as they migrate in a voltage field.

2.2.2 Steric Stabilization

Steric stabilization takes place when large molecules adsorb on to the surface of particles thus introducing physical barriers between them [20]. Stabilization is achieved by attaching or grafting of macromolecules to the surface of the particles (See fig 2.7).

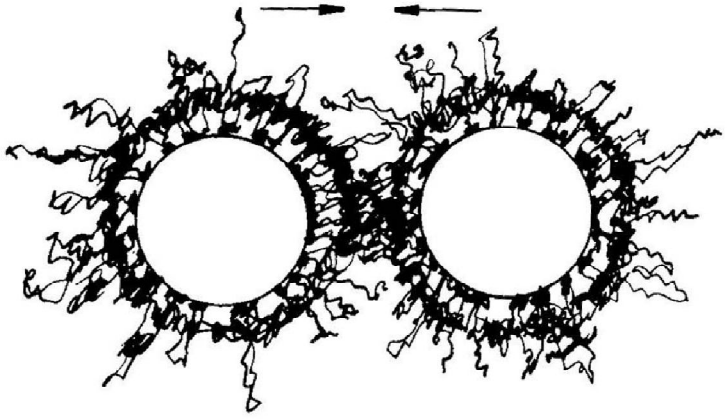

Fig 2.6: A schematic description of steric stabilization according to [12]

The point at which flocculation is first detected on decreasing the affinity of the dispersion medium for the stabilizing moieties is termed the *critical flocculation point (CFTP)*. The CFPT can therefore be used to evaluate the stability of the colloidal particles in steric stabilization. The CFTP can be influenced by the following system parameters: particle number concentration, the particle size, the nature of the anchor polymer, the surface coverage of the particles, the nature of the dispersed phase, the nature and molecular weight of the stabilizing moieties and the solvent.

2.2.2.1 Mechanism of Steric Stabilization

It is known that an interaction between layers take place when two particles with adsorbed polymer layers approach each other at a distance which is less than twice the thickness of the adsorbed layer. The degree of stabilization can thus be defined quantitatively in terms of Gibbs free energy change occurring upon the interaction of the adsorbed layers.

Mathematically, we define the Gibbs free energy change ΔG as:

$$\Delta G = \Delta H - T\Delta S \qquad (2.15)$$

where T is the temperature, ΔH is the enthalpy change and ΔS the entropy change.

A negative ΔG upon overlap of the adsorbed layers results in coagulation or flocculation. On the other hand, stabilization is achieved if ΔG is positive. It is therefore evident that stability depends on the change in enthalpy ΔH and entropy change ΔS.

Several theories have been proposed to explain the mechanism of steric stabilization and theoretical equations abound to calculate the energy change with the overlap of the adsorption layers. The entropic stabilization theory shall be discussed in this work

In the entropic stabilization theory, it is assumed that a second surface approaching the adsorbed layer cannot be penetrated. This result in the compression of the adsorbed layer and the polymers present in the interaction region lose configurational entropy. This implies that the polymer segments occupy fewer possible configurations in the compressed state than in the uncompressed state. This reduction in entropy increases ΔG, producing the net effect of repulsion between the particles and thus preventing the particles from flocculating. In the entropic stabilization theory, the enthalpic interaction between the adsorbed molecules and the dispersion medium is neglected so that $\Delta G = -T\Delta S$ [21].

In general, the advantages of steric stabilization over electrostatic stabilization include the following [22]:

- *Equal efficacy in both aqueous and non-aqueous dispersion media*: Charge stabilization is less effective in non-aqueous dispersion media than it is in aqueous media. This is primarily due to the low relative dielectric constant (<10) of most non-aqueous media. In contrast, steric stabilization is effective in both non-aqueous media and aqueous media. This explains why steric stabilization is usually preferred for non-aqueous dispersion media
- *Equal efficacy at both high and low solids content*: In charge stabilization in non-aqueous media, the thickness of the double layers can be so large, (due to the low dielectric constant of the dispersion medium), that the mere preparation of high solids dispersions forces the particles too close together which then leads to coagulation. In aqueous dispersion media, the preparation of charge-stabilized particles at high solids dispersions is often difficult because of the gel formation induced by the interactions between the double layers surrounding each particle.
- *Reversibility of flocculation*: The coagulation of charge-stabilized particles (induced by the addition of electrolyte) is usually irreversible by subsequent dilution. In contrast, flocculation of sterically stabilized dispersions (induced by the addition of a nonsolvent for the stabilizing moieties) can usually be reversed spontaneously by mere dilution of the

nonsolvent concentration to a suitably low value. This difference is due to the fact that sterically stabilized dispersions may be thermodynamically stable while charge stabilized dispersions are only thermodynamically metastable. As a consequence, for charge stabilized dispersions, the coagulated state represents a lower energy state and the coagulation can be reversed only after input of work into the system. Another important consequence of the thermodynamic stability of sterically stabilized dispersions is that they can redisperse spontaneously after drying.

2.3 Influence of process variables during Titanium (IV)-oxide nanoparticles synthesis

In previous works [23, 25], it has been demonstrated that the nature of properties of sol is influenced by the method of production and these properties (including structural and textural) can be modified by the growth process. Since there is no consensus in literature and no published standard by recognized standard organizations (such as the British Standards (BS), International Organization for Standardization (ISO) and the American Society for Testing Materials (ASTM) standards) for the optimum methodology for the preparation of Titanium (IV)-oxide sols, research groups have developed different preparation routes leading to sols with different properties in terms of particle size, concentration and stability. It has therefore become necessary to understand the influence of process variables in the production of these sols. An improved knowledge of the influence of process variables will allow for optimization of the material properties and a better control of the process kinetics.

Vorkapic and Matsoukas [24] found the optimum conditions for the production of TiO_2 particles by studying the effect of pH, temperature, length of the alkoxy group and long term stability.

Cordero-Cabrera et. al [20] also reported on the effect of temperature, water/alkoxide molar ratio, acid/alkoxide molar ratio ratio on the particle size and stabilization of Titanium (IV)-oxide sols using titanium tetraisopropoxide as a precursor.

A summary of relevant results obtained on the influence of these parameters are presented below:

2.3.1 Influence of Alkoxide types

Alkoxides are primarily formed as a result of reactions between highly reducing metals and alcohol. Vorkapic and Matsoukas [24] studied the influence of four alkoxides during the production of Titanium (IV)-oxide sols. The experiments were carried out at temperatures of 25°C and 50°C while keeping the temperature constant for each process. It was reported that

final size decreased in the order of increasing the length of the alkoxyl group at 25℃ while at 50°C the size decreased for all the four alkoxides. The influence of alkoxides is not significant but Titanium isopropoxide is preferred because of its high reactivity and low electronegative value of titanium. Titanium isopropoxide also had the best performance when compared to other alkoxides in the preparation of Titanium (IV)-oxide nanoparticles.

Cordero-Cabrera et. al [25] reported that water/alkoxide molar ratios ranging from 250 to 1000 and acid/alkoxide molar ratios ranging from 0.4 to 0.7 produced stable monomodal sols. The water/alkoxide ratio showed only a little influence on the results obtained.

2.3.2 Influence of pH values

In investigating the stability of Titanium (IV)-oxide sols, Cordero-cabrera et. al [25] reported on the influence of pH values on the results obtained. The stability of the sols was assessed by how thick a precipitate (if any) had formed on the bottom of the sample bottles after a five month period. Stable sols were produced after redispersion at 50^0C irrespective of the pH. At 70^0C stable sols were formed if the pH was below 1.7 and significant precipitation was observed under the two least acidic conditions used (Water/Alkoxide ratio of 1000 and the Nitric acid/Alkoxide ratio ≤ 0.5). The studies further revealed that a lower pH is required to maintain sufficient charge on the particles to keep them from agglomerating.

Smaller size particles are also obtained by the addition of acids during the hydrolysis rather than during redispersion [24]. The size of colloid formed is also sensitive to the amount of acid and the smallest particles were obtained when the $[H^+]$:[Ti] molar ratio was 0.2. The study further showed that when sols are peptized at 50^0C without the addition of alcohol and low $[H^+]$:[Ti] molar ratio are applied, TiO_2 aggregates were not redispersed due to insufficient acid while higher ratios have a notorious effect on the stability of the nanoparticles. The smallest particles are produced at $[H^+]$:[Ti] =0.5. This molar ratio was applied at the start of the reaction and produced a solution with a pH of 1.2. The suspension consists of small clusters that contain few primary particles at this pH [24].

The long term stability of the sol and size of the colloid after redispersion is also influenced by the addition of acid. Unstable sols are found at high molar ratio and stable ones at optimum molar ratios (0.5) after five days of experiment [24].

2.3.3 Influence of temperature

Cordero-Cabrera et. al [25] reported that the redispersion temperature is the parameter with the greatest significance. The results obtained agree with the famous DLVO theory that an

increase in redispersion temperature leads to an increase in the kinetic energy of the particles, increasing therefore the probability for them to collide and agglomerate. This is also in agreement with studies by Vorkapic and Matsoukas [24], though making a direct comparison of values is impossible as information on the polydispersity of the samples were not provided. The optimum temperature for the production of Titanium (IV)-oxide nanoparticles is found to be 50^0C. This was maintained at all times. Also, the size of the peptized colloid obtained at 50^0C from the propoxide, iso-propoxide and butoxide are in the range of 19-23 nm [24].

CHAPTER 3

CHARACTERIZATION OF TITANIUM (IV)-OXIDE NANOPARTICLES

The most important characteristics of a particle are its size, shape and density. For particles in the nanometer range, the determination of these characteristics becomes more challenging. This is because the particles produced during the synthesis of nanoparticles are not of single size. They range from primary particles to agglomerates of size several fold from the primary particles. Since there is no uniform law for the formation of particles during the agglomeration and breakage process, it is necessary to understand the average size of the particles and the distribution of the sizes about the average. The nature of this distribution is not only dependent on the random aggregation-breakage process but also on systematic influences. Hence, the need to understand the measurement of the particle size distributions of nanoparticles.

3.1 Particle size distribution (PSD)

The rate of formation of particles is essentially important in the determining the distribution in the size of particles during an agglomeration and redispersion process. A knowledge of the behaviour of these particles is important for understanding and optimisation of processes and operations [87].

Disperse systems consist of individual particles whose physical properties have to be characterised as precise as necessary, i.e. in process engineering these are so-called granulometric properties. Considering particulate solids as the material most commonly produced in particle technology, there is in many cases a very complex influence of the individual particle characteristics on the behaviour of the population as a whole, e.g. flow and compression behaviour of particle beds [87].

In this context, the particle size analysis is an important question. Experimental determination seems to be an easy thing to do, but especially for ultrafine and nanoscaled dispersed systems one should take into account critical aspects arising, e.g. from shape, concentration, interactions, and homogeneity effects of the particles. Likewise, experimental techniques available for particle sizing, e.g. image analysis, electron microscopy, light scattering, laser diffraction, and ultrasonic methods, use different physical theories in the background. The quantities of individual particles with a diameter d (the spherical shape is often the basic

assumption of the method) can be described mathematically with the help of cumulative particle size distributions.

For a continuous distribution, the cumulative distribution function $Q_r(d)$, is defined as the fraction of the total number of particles with diameters less than d. mathematically, this is shown as [87]:

$$Q_r(d) = \int_0^d q_r(d)d\,(d) \tag{3.1}$$

$$q_r(d) = \frac{dQ_r(d)}{d(d)} \tag{3.2}$$

Here, $q_r(d)$ is the particle size frequency distribution and the index r gives the quantity measured (e.g. number or mass based distributions).

The slope of the cumulative distribution function therefore helps to obtain the frequency function $q_r(d)$ at any point. Since the cumulative function is defined as the integral of the frequency function, it is less sensitive to scatter the data. This makes smoothing and interpolation of measurement results reliable. This makes the cumulative function more preferable over the frequency function.

3.1.1 Measurement of the PSD

Several instrumentations are available for the measurement of particle size distribution. The Mastersizer 2000 from the Malvern Company measures 20 nm to 2000 µm while the Zetasizer Nano from the same Company measures sizes between 0.6 nm – 6 µm. The Zetasizer Nano was used in this work. It is based on the principle of dynamic light scattering.

3.1.1.1 Dynamic Light Scattering

The Dynamic light scattering (also known as Photon Correlation spectroscopy) is one of the most popular techniques used in determining the size of particles. It is based on the principle that when a monochromatic light beam, such as a laser is shone on a solution of particles in random or Brownian motion, a Doppler Shift results when the light hits the moving particle. This results in a change of the wavelength of the incident light. The change in wavelength is related to the particle size by a computation of the sphere size distribution. It is also possible

to give a description of the particle's motion in the medium, measuring the diffusion coefficient of the particle and using the autocorrelation function.

The diameter that is measured in Dynamic Light Scattering is called the hydrodynamic diameter and refers to how a particle diffuses within a fluid. The technique measures the diameter of a sphere that has the same translational diffusion coefficient as the particle being measured.

As the dynamic light scattering method is automated, particle sizes can be measured in relatively short time and extensive experience is not required. The technique also offers a possibility to analyze samples containing broad distributions of species of widely differing molecular masses (e.g. a native protein and various sizes of aggregates), and to detect very small amounts of the higher mass species (<0.01% in many cases). The operation of the Zetasizer is based on the principle of dynamic light scattering.

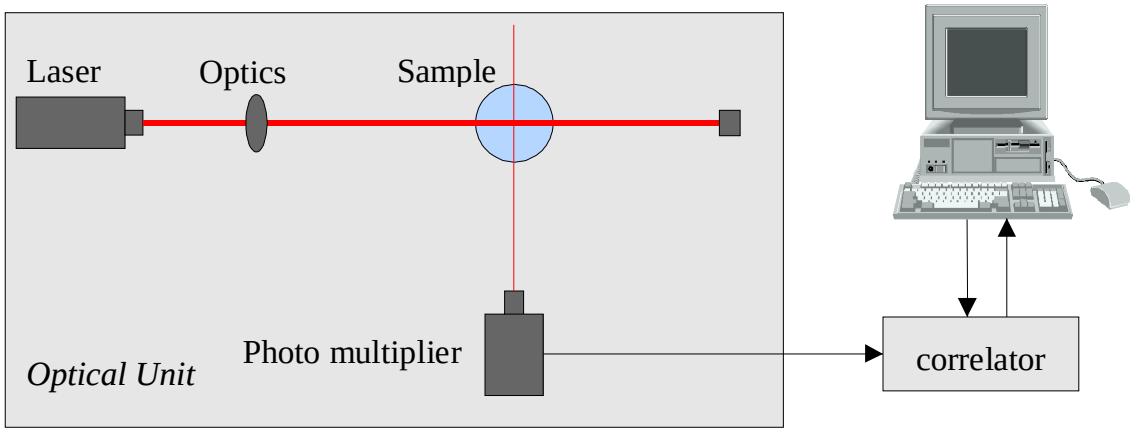

Fig. 3.1: A schematic representation of the principle of Dynamic Light Scattering

3.2 Stability of Titanium (IV)-oxide Nanoparticles

The electrostatic repulsion theory explains the stability of Titanium (IV)-oxide nanoparticles. The theory is based on the Helmholtz double layer approach. Ionic molecules adsorb on the solid particle and impart an ionic charge on the surface. As two particles approach, the electrostatic repulsive force is developed which leads to improved stabilization. The point zero charge value (the pH value at which the particle in the liquid medium a net zero charge on the surface) for Titanium (IV)-oxide was determined at a pH of 6.8. If the pH value is reduced slowly from the point zero charge value, it makes the surface potential much more

positively charged. The implication of this is that the Titanium (IV)-oxide particles become more positive and as a consequence attract negative ions inside the fluid to come around the particles. Since counter-ion positions have been filled in before (as pH reduced), the negative ions float around the area of electric double layer resulting in an increase in thickness, repulsion forces and consequently increased particle stability.

Nanocolloid Titanium (IV)-oxide is found to be stable at zeta potential ranges between +20mV and +40mV in dependency with pH values from 0.4 to 1.8 [28].

3.2.1 Zeta Potential Measurement

A classical microelectrophoresis system involves the application of a potential on electrodes fixed at two ends of a capillary cell. The velocity of particles is measured and expressed in unit field strength as they travel towards the electrodes [29].

Zeta Potential measurements are important in the determination of the nanoparticles produced. The commercial instrument used for measuring zeta potential is the Malvern Zetasizer Nanoseries. The equipment uses a combination of laser Doppler velocimetry and phase analysis light scattering to measure the particle electrophoretic mobility. This allows the accurate measurement of high conductivity samples and samples with low mobilities, such as particles dispersed in non-aqueous solvents. Low applied voltages also aids the avoidance risk of sampling effects due to Joule heating. Electrophoretic mobility refers to the velocity of a particle in a unit electric field or voltage gradient. The velocity is dependent on the strength of the electric field, the dielectric constant of the medium, the viscosity of the medium and the zeta potential [30, 31]. The relationship between zeta potential and electrophoretic mobility is given by:

$$\mu_E = \frac{\vec{V}}{\vec{E}} = \frac{2\varepsilon z\, \mathrm{f}(\kappa a)}{3\eta} \tag{3.3}$$

where μ_E is the electrophoretic mobility, z is the zeta potential, ε is the dielectric constant, η is the viscosity and $\mathrm{f}(\kappa a)$ is Henry's function.

A zeta potential measurement system comprises of six main components. Firstly, a laser provides a light source to illuminate the particles within the sample. For zeta potential measurements, this light source is split to provide an incident and reference beam. The incident laser beam passes through the centre of the sample cell, and the scattered light at an angle of about 13^o is detected. When an electric field is applied to the cell, any particles

moving through the measurement volume will cause the intensity of light detected to fluctuate with a frequency proportional to the particle speed and this information is passed to a digital signal processor and then to a computer. The Zetasizer Nano software produces a frequency spectrum from which the electrophoretic mobility and hence zeta potential is calculated. The intensity of the detected, scattered light must be within a specific range for the detector to successfully measure it. This is achieved using an attenuator, which adjusts the intensity of the light reaching the sample and hence the intensity of the scattering. To correct for any differences in the cell wall thickness and dispersant refraction, compensation optics are installed to maintain optimum alignment.

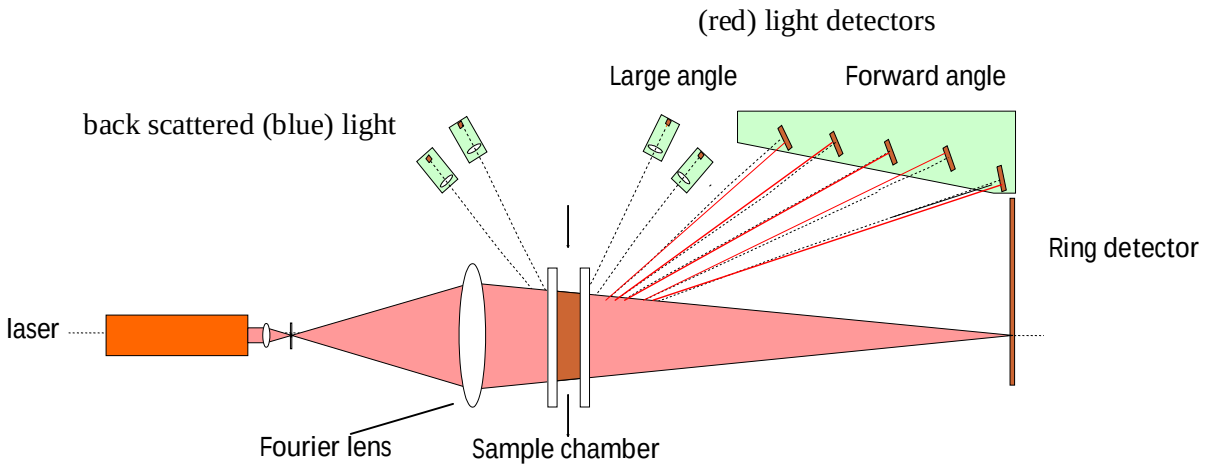

Fig. 3.2: Schematic representation of the Mastersizer 2000

3.2.2 Long-term Stability

The long-term stability of Titanium (IV)-oxide sols is dependent on the amount of acid present. Matsoukas et al. [24] noted a slow approach to steady state after 5 hours and 1 day of redispersion. They also noted the instability and tendency for reaggregation of several sols at high ratios of $[H^+]$: [Ti] after redispersion for 5 days. Bartlett and Woolfrey [88] obtained similar results. An optimum $[H^+]$: [Ti] ratio of 0.5 was used and no change was observed over a long period of time.

3.3 Morphology of Titanium (IV)-oxide Nanoparticles

A major problem encountered during the synthesis of nanoparticles is that a single production process may yield nanoparticles of varying size, shape, structure, and chemistry. These factors influence the observed properties of such nanoparticles and determine the success of nanoparticle-based devices [32]. These irregular shapes formed are called fractal objects, and they possess effective occupied volumes larger than the total volume of the primary particles.

The fractal dimension d_F is a measure of the compactness of agglomerates formed and relates to the mass of the particles formed thus [33]:

$$m \propto l^{d_F} \tag{3.4}$$

where l is the largest diameter of the irregular agglomerates and m is the mass of the particles. Hence, a low fractal dimension value results in a more open structure of the agglomerates. Since surface is so important for such small particles, it becomes important to know the forms and structures of the surfaces present in order to understand and model their properties. This is the basic aim of morphology studies. Theoretical and experimental studies have revealed that morphology is a function of particle size [34] and Titanium (IV)-oxide particles have been observed to take on spherical geometrical shapes [35] upon investigation.

The oldest and most highly developed technique for studying the structure and morphology of supported clusters is the transmission electron microscopy (TEM) [36]. Other techniques include X-ray photoelectron spectroscopy and scanning electron microscopy. The TEM has been discussed below.

3.3.1 Transmission Electron Microscopy

In the case of a transmission electron microscopy (TEM), a beam of electrons are focused on a single, pinpoint spot or element on the sample being studied. The electrons interact with the sample and only those that go past unobstructed hit the phosphor screen on the other side. At this point, the electrons are converted to light and an image is formed.

The dark areas of the image correspond to areas on the specimen where fewer electrons were able to pass through (either absorbed or scattered upon impact); the lighter areas are where more electrons did pass through, although the varying amounts of electrons in these areas enable the user to see structures and gradients.

The 'lenses' in a TEM are not the same as lenses in a conventional microscope; these are actually EM devices that can 'focus' the electron beam to the desired wavelength or size. In much the same way as a light microscope, however, the amount of power used to generate electrons allows for higher magnification or better resolutions.

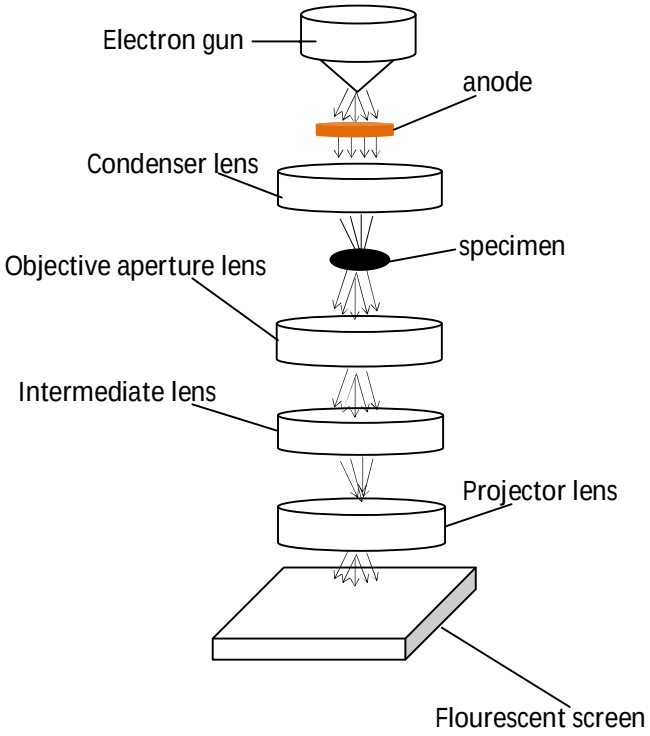

Fig. 3.3: Schematic representation of the transmission electron microscope

3.4 Specific Surface Area Measurement

The specific surface area is a measure of the total surface area per unit of mass. Specific surface area measurements are used by catalyst manufacturers to monitor the activity and stability of catalysts and they are measured by the use of nitrogen adsorption/desorption isotherms at liquid nitrogen temperature and relative pressures (P/P_0) in the range of 0.05 to 1.0. Hence, large uptakes of nitrogen at low relative pressures indicate the filling of the micropores in the catalyst.

The BET method [39] is one of the most popular and effective way of measuring the specific surface area of porous materials and it is discussed below.

3.4.1 BET Method

The BET method, elaborated by Brunauer, Emmett and Teller is a method of determining the specific surface area based on the phenomenon of physical adsorption of gases on the external and internal surfaces of a porous material [37].

The amount of gas adsorbed is dependent on the relative vapour pressure and proportional to the total external and internal surface of the material. The relationship between the relative vapour pressure and amount of adsorbed gas at constant temperature is called the adsorption isotherm [37]. The gases used as adsorptives have to be only physically adsorbed by weak bonds at the surface of the solid (van der-Waals forces) and can be desorbed by a decrease of pressure at the same temperature. The most common gas is nitrogen at its boiling temperature (77.3 K). In the case of a very small surface area (below 1 m^2/g), the sensitivity of the instruments using nitrogen is insufficient and krypton at 77.3 K should be used [38].

In determining the adsorption isotherm volumetrically, the sample is dried and outgassed through heating under vacuum. Thereafter, specific amounts of adsorptive are passed into the sample cell. The difference between the amount of gas admitted and the amount of gas filling the free space in the sample cell including connections gives the amount of gas adsorbed. The adsorption isotherm is obtained by plotting the amount gas adsorbed (in mol/g) as a function of the relative pressure (p/p_0). A linearized form of the BET equation is thus defined as [87]:

$$\frac{p}{V_{ads} \cdot (p_0 - p)} = \frac{1}{V_{mono} \cdot C} + \frac{(C-1) \cdot p}{V_{mono} \cdot C \cdot p_0} \tag{3.5}$$

Where V_{ads} is the adsorbed amount of gas at a relative pressure p/p_0 and V_{mono} is the adsorbed amount of monolayer capacity. C is a constant related to the adsorption enthalpy (bond energy of adsorbate molecules. If the linearized equation is plotted, we obtain:

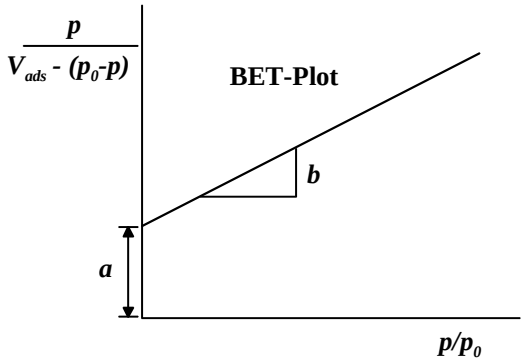

Fig.3.4: Linearized form of the BET equation according to [87].

The intercept *a*, and the slope *b*, must be positive and are determined by linear regression. The relative pressure range should be within 0.05 and 0.3. From these values, the monolayer capacity (in mol/g) can be calculated according to V_{mono} = 1/(a+b) where:

$$a = \frac{1}{V_{mono} \cdot C} \tag{3.6}$$

$$b = \frac{(C-1)}{V_{mono} \cdot C} \tag{3.7}$$

If we assume that there is only one monolayer of nitrogen gas (cross sectional area for nitrogen gas A_{N_2} is known with 0.162 nm^2) completely covering the particle surface, the BET surface area A_{BET} can be calculated as [87]:

$$A_{BET} = \frac{V_{mono} \cdot N_L \cdot A_{N_2}}{V_{mol}} \tag{3.8}$$

where N_L is the Avogardo constant and V_{mol} is the molar gas volume (22.4L/mol).

CHAPTER 4

MODELS FOR AGGLOMERATION AND REDISPERSION KINETICS

Particulate processes are characterized by the presence of a continuous phase and a dispersed phase composed of particles with a distribution of properties. These particles, depending on the process, exist in forms of crystals, grains, drops or bubbles and may have different properties relating to their size, composition, porosity and enthalpy [40]. In several applications, the size of these particles is used to characterize a particle due to the ease of measurement when compared with other properties and the possibility of determining it in several forms ranging from length, mass, area to volume [40].

A mathematical description of the distribution of this particle property becomes necessary since different sizes and properties may exist. The shape of particles is often uniform enough that a characteristic shape factor can be defined and the particles can thus be described using the one-dimensional distribution function [40].

Population balance models are used to describe the property of particles that are distributed according along a certain coordinate of property. These models include conventional material and energy balance (which represents birth and death of members) and an internal realignment component to account for drifts in population of members from one age to the other. This will be discussed in more details later.

4.1 Particle formation mechanisms

These properties of these particles change in a system due to several mechanisms. The most common mechanisms are aggregation, breakage, nucleation and growth. For the purpose of this work, we shall focus on aggregation and breakage alone.

4.1.1 Agglomeration

Agglomeration involves the formation of a large particle when two or more particles collide together. The distinct feature of the agglomeration mechanism is the conservation of mass with a reduction in the total number of particles. The process is common in powder processing industries where dust is undesirable and also in fluidized bed systems. Agglomeration of small dust particles improves the handling properties and reduces risks of

dust explosions. Agglomeration also leads to higher dissolution rate by minimizing lump formation or flotation of powders.

Agglomeration of liquid droplets is known as coagulation. In coagulation, the original droplets cannot be distinguished from the newly droplets. In the case of solids, the original particles stay intact [40, 41].

Several theoretical models are available for estimating the probability that two colliding particles will stick together or not. A wide range of assumptions are made about the mechanical properties of the particles and the system characteristics.

4.1.2 Breakage

During a breakage process, particles split into two or more fragments. This leads to a significant increase in the number of particles while the total mass is conserved (remains constant or unchanged).

Two cases are considered in granule breakage – breakage of wet granules in the granulator and fracture of dried granules in the granulator or in subsequent handling. Breakage of wet granules will influence and may control the final granule size distribution, especially in high shear granulators [40].

Breakage can be applied in cases where limits have to be placed on the maximum granule size or where a viscous binder has to be distributed. This has a tendency to increase the rate at which dusty fines are produced and thus increase risks of explosions and increase handling and storage costs.

The breakage process is also referred to as fragmentation or reversible agglomeration depending on the process used.

4.1.3 Growth

In a Growth process, the number of particles remains constant but the total volume of particles increase. Growth (also known as layering or coating) takes place when a non-particulate matter adds to the surface of a particle leading to a continuous increase in the size of the particles. A typical example is found in fluidized systems where a liquid is sprayed on solid particles with the aid of nozzles in the form of drops. The surrounding gas stream produce intensive heat and mass transfer which results in a rapid increase of hardness of the

fluid film through drying, if the initial product is in a molten state, or through cooling, if the product sprayed upon is melted.

4.1.4 Nucleation

Nucleation involves the formation of new particles by condensation of non-particulate matter. The nucleation process has a significant effect on the total number of particles but the effect on the total volume of particles is much less. In nucleation, the nuclei are usually treated as the smallest particle in the system [40].

4.2 Rates of the agglomeration and redispersion process

Population balance models are used to describe the dynamic evolution of the distribution of one or more properties in agglomeration and redispersion problems. Since the rates of these processes are not equal, the average size of the aggregates either increase or decrease depending on the dominant mechanism. The steady state is defined as a stage where a dynamic equilibrium exists between the agglomeration and redispersion process. The rate of agglomeration is dependent on two factors – the rate at which collision takes place and the probability of cohesion after collision. On the other hand, the redispersion process is dependent on fluid shear and probability of redispersion after collision. The rate equation describing the rate of change of particles is given as:

$$\frac{dC_n}{dt} = \frac{1}{2}\sum_{i+j\to k} \alpha\, \beta_{ij} C_{ni} C_{nj} - \sum_{n=1}^{\infty} \propto \beta_{ik} C_{ni} C_{nk} - S_n C_n + \sum_{n=1}^{\infty} \gamma_{n,j} S_j C_{nj} \qquad (4.1)$$

Where, C_n is defined as the number concentration of the agglomerate of size k (a single agglomerate contains k number of primary particles), $\propto$ is the fraction of collision resulting in agglomeration (called the collision efficiency), β_{ij} is the collision frequency for particles of volume i and volume j. S_n is the breakage or redispersion rate of agglomerates of size k and $\gamma_{n,j}$ is the breakage distribution function defining the volume fraction of the fragments of size n originating from the j-sized particles.

The first term on the right hand of the above equation is the number increase of k –size particles by i and j particles. The second accounts for the formation of large agglomerates due to the loss of k-size agglomerates. The factor $1/2$ is added to make sure that the above combination cannot be counted twice. The third term refers implies the loss of n-size

agglomerates due to the redispersion process and the fourth term indicates the formation of the n-size agglomerates by the death of large agglomerates [42].

Under constant shear, the particle size distribution observed arises from the initial distribution which at t=0 consists fully of primary particles. While the number of agglomerates of a certain sixe can be reduced by agglomeration to larger agglomerates and also by redispersion to small particles, the number of primary particles is through the breakage of aggregates [42].

4.3 Formulation of the Population Balance Equations to describe the kinetics of a agglomeration and redispersion kinetics

4.3.1 Birth term B_{Agg} of the Agglomerate of Size *k*

The process of an agglomeration birth for a di-mer is depicted in Fig. 4.1 below. If we assume that an agglomerate of size *k* is formed from agglomerates of size *i* and *k-i*, then there are two reaction possibilities:

$$i - mer + (k - i) - mer \xrightarrow{k_{i,k-i}} k - mer \tag{4.2}$$

$$(k - 1) - mer + i - mer \xrightarrow{k_{k-i,i}} k - mer \tag{4.3}$$

The two possibilities above result in the formation of a product of particle size *k*. We can therefore express the kinetics of the agglomeration for both processes as:

$$\frac{dC_{nk}}{dt} = k_{1,k-1}C_{k1}C_{nk-1} \quad \dots \qquad \dots \quad \frac{dC_{nk}}{dt} = k_{k-1,1}C_{nk-1}c_{n1}$$
$$\frac{dC_{nk}}{dt} = k_{2,k-1}C_{n2}C_{nk-2} \quad \dots \qquad \dots \quad \frac{dC_{nk}}{dt} = k_{k-2,2}C_{nk-2}C_{n2} \tag{4.4}$$

These possibilities are valid until the condition $i \neq k - i$ is satisfied. This can be expressed as:

$$1 - mer + (k - 1) - mer \Leftrightarrow (k - 1) - mer + 1 - mer$$
$$2 - mer + (k - 2) - mer \Leftrightarrow (k - 2) - mer + 2 - mer \tag{4.5}$$

To ensure that the expression is not counted twice, a factor of $^1/_2$ is introduced into the classical expression term as follows:

$$\frac{dc_{nk}}{dt} = \frac{1}{2}\sum_{i=1}^{k-1} k_{i,k-1} c_{ni} c_{n,k-1} \tag{4.6}$$

A factor (the Kronecker-Delta fuction) is introduced to represent two possibilities ($i = k - i$ and $i \neq k - i$) due to the collision of the particle sizes *i* and *k-i*. We can therefore present the conditions as follows:

$$\begin{aligned} i = k - i &\rightarrow \delta_{i,k-i} = 1 \\ i \neq k - i &\rightarrow \delta_{i,k-i} = 0 \end{aligned} \tag{4.7}$$

with the following possibilities:

$$\begin{cases} 1 - mer + 3 - mer \Leftrightarrow 3 - mer + 1 - mer \Rightarrow Factor: ½ \\ \\ 2 - mer + 2 - mer \qquad\qquad\qquad \Rightarrow Factor: 1 \end{cases} \tag{4.8}$$

We can therefore present the birth term for the agglomeration for an agglomerate of size *k* as:

$$B_{Agg} = \frac{1}{2}\sum_{i=1}^{k-1} (1 + \delta_{i,k-1}) k_{i,k-1} c_{ni} c_{nk-i} \tag{4.9}$$

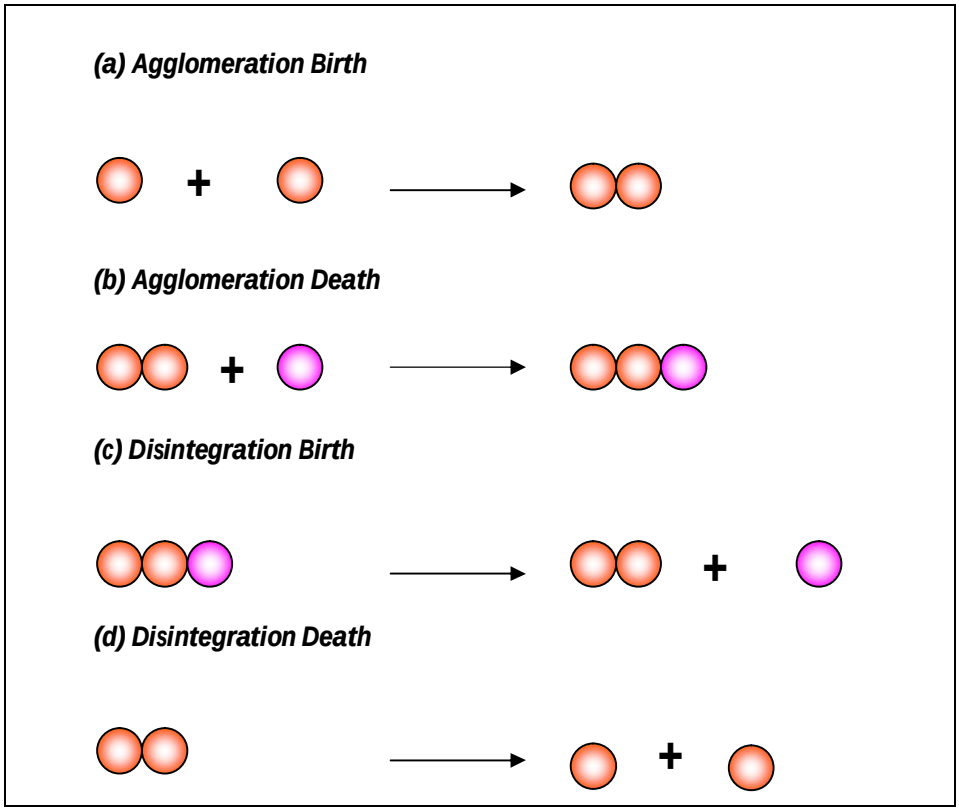

Fig. 4.1: Process of agglomeration and disintegration for a dimer

4.3.2 Death term D_{Agg} of the Agglomerate of Size *k*

The death term of agglomeration *(D_{Agg})* (illustrated in Fig.4.1 above) is the formation of an agglomerate greater than the agglomerate size *p* by the collision with the primary particles of size *i*, where *i=1, 2, 3…N_{max}* (N_{max} is the maximum number of primary particles in an aggregate) [42].

From the kinetic theory, we can represent the change in the concentration of the agglomerates of size n_{1+k} as [42]:

$$\frac{dC_{n1k}}{dt} = k_{1k} C_{n1} C_{nk} \tag{4.10}$$

For the maximum number of primary particles, $N_{max,}$ we have:

$$\frac{dC_{n2k}}{dt} = k_{2k} C_{n2} C_{nk} \ldots . \quad \ldots . \quad \frac{dC_{nN_{max,k}}}{dt} = k_{N_{max,k}} C_{nN_{max}} C_{nk} \tag{4.11}$$

When the agglomerates, composing of the primary particles are of the same size, such that, *i=k*, then $i - mer + k - mer \xrightarrow{k_{ik}} (i + k) - mer$. For *i=k*, we have, $2k - mer \xrightarrow{k_{ik}} kk - mer$.

A stoichiometric factor of $v_j = 2$ is multiplied in the rate expressions

$$\frac{dC_{nik}}{dt} = 2k_{ik}c_{ni}c_{nk} \tag{4.12}$$

The rate expression for the condition of the primary particle $i \neq p$ is written as:

$$\frac{dC_{nk}}{dt} = C_{nk} \sum_{\substack{i=1 \\ i \neq k}}^{N_{max}} k_{i,k}\, c_{ni} \tag{4.13}$$

The Kroeneker – Delta function explains why the equation for the condition $i=k$ above was multiplied by 2 as,

$$i = k \rightarrow \delta_{i,k} = 1$$
$$i \neq k \rightarrow \delta_{i,k} = 0 \tag{4.14}$$

The death term (D_{Agg}) for the particle size k of the agglomeration process is written as:

$$D_{Agg} = c_{n,k} \sum_{i=1}^{N_{max}} (1 + \delta_{i,k}) k_{i,k} C_{n,i} \tag{4.15}$$

Where,

$c_{n,k}$: the concentration of agglomerate comprising of k(=i+j) primary particles.

N_{max}: the maximum number of the primary particle i in the agglomerate

$k_{i,p}$: the agglomeration rate constant

In general, the PBE for the dynamic changes in the concentration of the particle size k due to the agglomeration process is given by the expression [42]:

$$\frac{dC_{nk}}{dt} = \frac{1}{2}\sum_{i=1}^{k-1} (1 + \delta_{i,k-1})\, k_{i,k-1} C_{ni} C_{nk-1} - C_{n,k} \sum_{i=1}^{N_{max}} (1 + \delta_{i,k})\, k_{i,k} C_{n,i} \tag{4.16}$$

4.3.3 Birth term B_{Redis} of the Agglomerate Size k due to Redispersion

Redispersion involves the formation of the agglomerates of size p by the destruction of the agglomerates of size greater than p. The kinetic expressions for the reaction are shown below:

$$\frac{dC_{nk}}{dt} = b_{1k}C_{n1+k}$$

$$\frac{dC_{nk}}{dt} = b_{2k}c_{n2+k}$$

: (4.17)

:

$$\frac{dC_{nk}}{dt} = b_{i-1,k}C_{n(i-1)+k}$$

The kinetic expression above can be written as follows if the size of the particles formed, *k* and i are the same:

$$\frac{dC_{nk}}{dt} = 2b_{ik}C_{ni+k} \quad (4.18)$$

The factor 2 is added for the stoichiometric coefficient v_p

If $i \neq k$, the equation becomes:

$$\frac{dC_{nk}}{dt} = \sum_{i=1}^{N_{max}} b_{ik}C_{ni+k} \quad (4.19)$$

Two conditions are made with the Kronecker –Delta function. The birth term for the redispersion B_{Redis} of the agglomerate of size *k* is given as:

$$B_{Redis} = \sum_{i=1}^{N_{max}} (1 + \delta_{ik})b_{ik}C_{n(i+k)} \quad (4.20)$$

4.3.4 Death term D_{Red} of the Agglomerate Size *k* due to Redispersion

The death of an agglomerate of size *k* can be represented by:

$$k - mer \xrightarrow{bi,k-i} i - mer + (k - i) - mer \quad (4.21)$$

The agglomerate of size *k* breaks into the particles of size *i* and *k*-*i*, with *i*=1, 2…*k*-1 making the formation of the nanoparticles as a dynamic process. The kinetic equations for the reaction can be given by the following sequence:

$$-\frac{dC_{nk}}{dt} = b_{1,k-1}C_{nk}$$

$$-\frac{dC_{nk}}{dt} = b_{2,k-2}C_{nk}$$

: (4.22)

:

$$-\frac{dC_{nk}}{dt} = b_{i-2,2}C_{nk}$$

$$-\frac{dC_{nk}}{dt} = b_{i-1,1}C_{nk}$$

The kinetic expression resulting from the break-up of particles of size *k* is given by:

$$-\frac{dC_{nk}}{dt} = \sum_{i=1}^{k-1} b_{i,k-i}\, C_{nk} \quad (4.23)$$

The problem under consideration is similar to the agglomeration kinetics with two possibilities, when $i \neq k - i$

$1 - mer + (k-1) - mer \Leftrightarrow (k-1) - mer + 1 - mer$
$2 - mer + (k-2) - mer \Leftrightarrow (k-2) - mer + 2 - mer$

A factor of ½ is multiplied in the kinetic expression to ensure for the condition of not accounting for the two possibilities. Hence, the expression becomes:

$$-\frac{dC_{nk}}{dt} = \frac{1}{2}\sum_{i=1}^{k-1} b_{i,k-i}\, C_{nk} \quad (4.24)$$

The Kronecker – Delta function represents the two possible particle split-ups, hence the birth term for particles of size *k* is given by:

$$D_{Redis} = \frac{1}{2} C_{nk} \sum_{i=1}^{k-1} (1 + \delta_{i,k-i})\, b_{i,k-i} \quad (4.25)$$

If the birth and death terms are added, the redispersion equation becomes”

$$\frac{dC_{nk}}{dt} = -\frac{1}{2}C_{nk}\sum_{i=1}^{k-1}(1+\delta_{i,k-i})\,b_{i,k-i} + \sum_{i=1}^{N_{max}}(1+\delta_{i,k})\,b_{i,k}C_{n(i+k)} \tag{4.26}$$

Finally, the overall discrete PBE for the simultaneous agglomeration and redispersion with the addition of the birth and death terms becomes;

$$\begin{aligned}\frac{dC_{nk}}{dt} = {} & \frac{1}{2}\sum_{i=1}^{k-1}(1+\delta_{i,k-i})\,k_{i,(k-i)}C_{ni}C_{n(k-i)} - C_{n,k}\sum_{i=1}^{N_{max}}(1+\delta_{i,k})\,k_{i,k}C_{n,i} \\ & -\frac{1}{2}C_{nk}\sum_{i=1}^{k-1}(1+\delta_{i,k-i})\,b_{i,k-i} \\ & +\sum_{i=1}^{N_{max}}(1+\delta_{i,k})\,b_{i,k}C_{n(i+k)}\end{aligned} \tag{4.27}$$

4.4 Overview of relevant kernels for agglomeration and redispersion kinetics

An overview of agglomeration and redispersion kernels is presented below.

4.4.1 Agglomeration Kernels

The mathematical representation of agglomeration has been based on the consideration that the process consists of two discrete steps: transport and attachment. The transport step, which leads to the collision of two particles, is achieved by the virtue of the local variations in fluid/particle velocities arising through-

(1) Imposed velocity gradients from mixing (Orthokinetic agglomeration)
(2) The random thermal 'Brownian' motion of the particles (Perikinetic agglomeration)
(3) Differences in the settling velocities of the individual particles (differential sedimentation).

On the other hand, attachment is dependent upon a number of short-range forces largely pertaining to the nature of the surface themselves [43].

The fundamental assumption of the aggregation process is that it is a second-order rate constant process in which the rate of collision is the product of concentrations of the two

colliding particles. Mathematically, the rate of successful collision between particles of size i, j is given by,

$$Rate\ of\ collision = \alpha\beta(i,j)C_{ni}C_{nj} \tag{4.28}$$

Where, α as defined before is the collision efficiency, $\beta(i,j)$ is the collision frequency between particles of size i, j and C_{ni} and C_{nj} are the particle concentrations for particles of size i, j, respectively.

The collision frequency β is a function of the method of aggregation, i.e. Perikinetic, Orthokinetic or differential sedimentation. The collision efficiency, α (values from 0 to 1) is a function of the degree of the particle destabilization. The value of α increases as the degree of destabilization increases. Thus, in effect, β is a measure of the transport efficiency leading to collisions, while α represents the percentage of those collisions, which results in successful collisions. All the models are based on this fundamental equation. The values of the parameters α and β depend upon the nature of particles to the methods of destabilization and the flow regime during aggregation.

Also the importance of C_{ni} and C_{nj} are noted. The overall rate increases with particle concentration. Despite the theoretical difficulties, the basic assumption is that the collision rate is independent of the colloidal interactions and depends only on particle transport.

The assumption is based on the short-range nature of interparticle forces, which is usually much less than the particle size, so that the particles come in contact before these forces play a role. The decoupling of transport and attachment steps is a great simplification in the aggregation kinetics. At the moment, let us assume that every collision between the particles results in the formation of an aggregate (i.e. the collision efficiency, $\alpha = 1$. Hence, the collision rate constant and the aggregation rate constant are the same. Particle aggregation can be described as by the rate at which a certain size aggregate is being formed by smaller aggregates minus the rate at which the aggregate combines to form a larger aggregate from small aggregates.

The Smoluchowski equation shows the rate of change of concentration of *k*-fold aggregates, where $k = i + j$, below [56] :

$$\frac{dC_n}{dt} = \frac{1}{2}\sum_{\substack{i+j\to k \\ i=1}}^{i=k-1} \beta_{i,j} C_{ni} C_{nj} - C_{nk} \sum_{i=1}^{\infty} \beta_{i,k} C_{ni,} \tag{4.29}$$

Where, i, j and *k* represent particle sizes. The first term on the right hand side represents the rate of formation of *k*-fold aggregates such that the total volume is equal to the volume of the particle of size *k*. The summation by this method means counting each collision twice and hence the factor ½ is included. The second term on the right hand side describes the loss of particles of size *k* by virtue of their aggregation with other particle sizes. The notable point is that the above equation is applicable only for irreversible aggregation since no term is included for the break-up of the aggregates, which is usually common in aggregating environments.

4.4.2 Redispersion Kernels

Disintegration is usually first order with respect to particle concentration, since it does not generally depend on collisions but on the local hydrodynamic field acting on the particles. One of the assumptions in Smoluchowski theory is that the agglomerates do not break when once formed. However, it is the balancing of opposing phenomena of agglomeration called redispersion that decides the agglomerate size and mass distribution. Computer simulations have showed the importance of redispersion or breakage in the agglomeration modeling [44]. Different researchers have proposed different disintegration function $b(t, r_i, r_j)$ or probability density function. The particle agglomeration and breakage based on a series of different simplified kernels assumes that the initial particle size distribution is monodispersed. The results show that the different assumptions can have effect on both the initial rates of reaction and the steady state concentrations [45]. The selection function (disintegration probability) is defined as [84]:

$$S(t, r_j) = S_0(t) r_j^{\mu} \tag{4.30}$$

where S_0 and μ are constant.

The Selection rate for disintegration S_n has been use for flow strain rate as the primary breakup parameter. The break up rate coefficient can be expressed as (Kramer and Clark 1997),

$$S_n = A(\dot{\gamma})^b (r_k)^a \ . \quad (4.31)$$

The term S_n is the selection rate for disintegration, A is the disintegration rate constant, b is breakup rate exponent, a is an aggregate size exponent and $\dot{\gamma}$ is the flow strain rate. This shows that the selection rate for disintegration is a function of flow strain rate resulting from energy input and the geometric properties of the agglomerate (i.e. Size, area, or volume).

Over the last many years several attempts have been made to model disintegration kernel. Disintegration kernels and selection functions are usually semiemprical. Disintegration kernels available include the Austin kernel, the Diemer kernel [49], Kramer kernel [50], exponential kernel [51], power law kernel [52], konno kernel [53] and the Sathyagal & Ramkrishna kernel [54] among others.

In the sections that follow, the Austin and Diemer kernel are discussed as these kernels were applied in the current study.

4.4.2.1 Austin Kernel

In a disintegration process, particles are stressed and may break into two or many fragments.

The disintegration distribution functions are usually semiemprical. Disintegration has a significant effect on the number of particles. The total number of particles in disintegration process increases while the total mass remains constant. The primary cumulative disintegration distribution function has the form first proposed by Austin as in *Eq. 4.32* below:

$$B(t, r_i, r_j) = \begin{cases} \emptyset \left(\frac{r_i}{r_j}\right)^{\gamma} + (1-\emptyset)\left(\frac{r_i}{r_j}\right); & r_j > r_i \\ 1 \quad ; & r_j = r_i \end{cases} \quad (4.32)$$

Where, ϕ, λ, γ are dimensionless material constants. It is clear that the value of the intercept increases with decreasing particle sizes. For the numerical simulation the disintegration kernel, $b(t, r_i, r_j)$ is used rather than cumulative kernel$B(t, r_i, r_j)$. The following selection function has been used for simulation.

$$S(t, r_j) = S_0(t)(r_j)^{\mu} \tag{4.33}$$

4.4.2.2 Diemer Kernel

There are several forms like binary disintegration (two fragments), ternary disintegration (three fragments) and normal disintegration where the aggregates are distributed in lower size ranges. It has been showed that binary disintegration function is easy to implement and can be comfortably applied to predict the average aggregate sizes, without the additional requirement of fitting coefficients [56].

Here we employed Diemer's generalized form of Hill and Ng's power-law breakage distribution [49] as in *Eq. 4.34* below

$$b(t, r_i, r_j) = \frac{\left(p(r_i)^c (r_j - r_i)^{(c+(c+1)(p-2)}\right)[c + (c+1)(p-1)]!}{(r_j)^{(pc+(p-1))}(c!)[(c + (c+1)(p-1))]!} \tag{4.34}$$

Where the exponent p describes the number of fragments per disintegration event and $c \geq 0$ determines the shape of the daughter particle distribution.

4.5 Methods of Solving population balance equations

Since Smoluchowski [56] put forward the population to study the mathematical theory of coagulation kinetics of colloidal solutions, population balance equations (PBE) has been considered the most powerful tool in the analysis of those systems composed of countable entities [56, 57, 58].

In general, methods of solving PBEs are grouped into four classes as follows [58]:

1. Analytical methods (which includes analytical solutions and similarity solutions) as seen in Kapur [59]; Ramabhadran and Seinfeld [60]; Das *et al*. [61]; Guilhem and Ring [62]; McGrady and Ziff [63]; Lui and Thompson [64].
2. The method of moments as seen in Argyiou *et al.* [65]; Hashimoto and Silveston [66]; Kane *et al* [67], Randolph and White [68]; Byrd and Mulligan [69].

3. Method of weighted residuals (MWR) as seen in Ramkrishna [18], Singh and Ramkrishna [70], Bhatia and Chakraborty [71], Chen *et al* [72].
4. Other methods such as the finite-element method (Frymier *et al.* [73], Nicmanis and Hounslow [74]), the method of direct discretization (Marchal *et al.* [75]) and the Cell Average Technique (CAT) [40].

In this work, the cell average Technique (CAT) is employed in solving the population balances and it is discussed below.

4.5.1 The Cell Average Technique

The cell average technique (CAT) is a new discretization method for solving one dimensional population balance problems [84].

This method approximates the number density in terms of Dirac point masses and is based on an exact prediction of some selected moments to solve the population balance equation. The aim of the cell average technique is to divide the entire size domain into a finite number of cells. The lower and upper boundaries of the ith cell are denoted by $x_{i-1/2}$ and $x_{i+1/2}$, respectively and $i = 1, \dots, I$ with $x_{1/2} = 0$ and $x_{I+1/2} = x_{max}$. All particles belonging to a cell are identified by a representative size in the cell, also called grid point. The representative size of a cell can be chosen at any position between the lower and upper boundaries of the cell. A typical discretized size domain is shown in *Fig. 4.2* below. The representative of the *i* cell is represented by $x_i = (x_{i-1/2} + x_{i+1/2})/2$. This is called the pivot. The width of the ith cell is denoted by $\Delta x_i = x_{i+1/2} - x_{i-1/2}$. The size of a cell can be fixed arbitrarily depending upon the process of application. In most applications, however, geometric type grids are preferred [40].

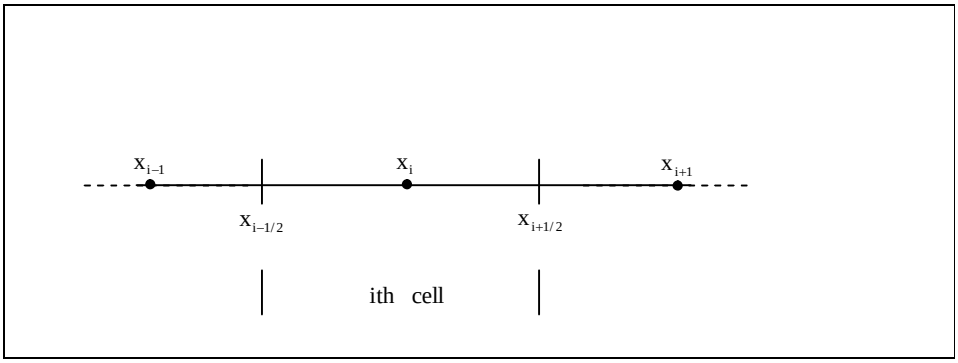

Fig. 4.2: A discretized size domain

It should also be noted that the points selected in the grid will be the points where the particle distributions are considered to be represented by a point mass. They can also be seen as the quadrature points using the mid-point rule, which is of second order. The total number of particles in a cell is defined as follows [84]:

$$N_i(t) = \int_{x_{i-1/2}}^{x_{i+1/2}} n(t,x)dx, \quad i = 1, \dots, I \tag{4.35}$$

If the truncated solution of the disintegration population balance equation [86] is integrated over each cell, and then discretizing as well as modifying the integrated birth term, we obtain the following cell average formulation for disintegration [84]:

$$\frac{dN_i}{dt} = B_i - D_{i,} \quad i = 1, \dots, I. \tag{4.36}$$

The terms B_i *and* D_i represent the birth and death rates of the particles in the cell i due to disintegration, respectively. The term B_i is given as:

$$B_i = B_{i-1}\lambda_i^-(\bar{v}_{i-1})H(\bar{v}_{i-1} - x_{i-1}) + B_i\lambda_i^-(\bar{v}_i) + H(x_i - \bar{v}_i) + B_i\lambda_i^+(\bar{v}_i)H(\bar{v}_i - x_i) + B_{i+1}\lambda_i^+(\bar{v}_{i+1})H(x_{i+1} - \bar{v}_{i+1}) \tag{4.37}$$

Where the Heaviside step function H is a discontinuous function and defined as [84]:

$$H(x) = \begin{cases} 1, & x > 0, \\ \frac{1}{2}, & x = 0, \\ 0, & x < 0. \end{cases} \tag{4.38}$$

The function used for the distribution of particles is given as:

$$\lambda_i^{\pm}(x) = \frac{x - x_{i\pm1}}{x_i - x_{i\pm1}} \tag{4.39}$$

and the volume average of incoming particles is calculated as:

$$\bar{v}_i = \frac{V_i}{B_i} \tag{4.40}$$

The totals of discrete birth B_i and death D_i due to disintegration are computed by the following expressions:

$$B_i = \sum_{k \geq i} N_k(t) S_k \int_{x_{i-1/2}}^{p_k^i} b(t, x, x_k) dx, \tag{4.41}$$

and

$$D_i = S_i N_i(t). \tag{4.42}$$

The notation S_i is used for $S(t, x_i)$ and the limit p_k^i is given by:

$$p_k^i = \begin{cases} x_i & if\ k=1 \\ x_{i+1/2} & otherwise \end{cases} \tag{4.43}$$

The discrete volume flux due to disintegration is given by:

$$V_i = \sum_{k \geq 1} N_k(t) S_k \int_{x_{i-1/2}}^{p_k^i} x b(t, x, x_k)\, dx \tag{4.44}$$

The set of Eq. (4.36) together with an initial condition $N_i(0), i = 1, \dots, I$, from Eq. (4.35) can be solved with any higher order ODE solver to obtain the total number of particles in each cell. It has been shown that the cell average scheme provides a significant improvement in predicting the particle size distribution in comparison to the other numerical schemes. The technique also allows the convenience of using non-homogenous, geometric or equal size cells. Moreover, the cell average technique enjoys the major advantage of simplicity for solving combined problems over other existing schemes [84].

For a more detailed description of the CAT scheme, readers are referred to see [40, 76]. In the next chapter we discuss the numerical simulation by using the cell average technique and comparing it with the experimental results.

CHAPTER 5

RESEARCH METHODOLOGY

This chapter describes the experimental set-up and methodology used in the sol-gel production of Titanium (IV)-oxide nanoparticles.

5.1 Experimental Set-up and Procedure

The production of Titanium (IV)-oxide nanoparticles on the laboratory scale using the sol gel technique took place in a reactor. The reactor (in our case, a beaker) was kept inside a temperature bath and maintained at a constant temperature of 50°C. This temperature is has been reported as the optimum during the production of Titanium (IV)-oxide sols [25]. The organic precursor used was titanium tetraisopropoxide (TTIP), $Ti(OC_3H_7)_4$ (97% produced by Alfa Aesar, Johnson and Matthey GmbH, Germany) and 0.1 M HNO_3 (Nitric acid)as used as the solvent. Stirrers with different impeller geometries (pitched blade and crossed blade) were also employed to mix the contents of the reactor in order to achieve homogeneity and aid to the kinetics of the synthesis.

The experiment commenced with 140 ml Nitric acid in the reactor and a stirrer shear rate $\dot{\gamma}$ =350 s^{-1} (corresponding to a stirrer rotational speed of 500 rpm). 9.8 ml of TTIP was later injected into the nitric acid solution resulting in rapid agglomeration as revealed by the rapid increase in turbidity and the formation of large visible agglomerates. Samples are taken periodically (basically on an hourly basis) using a syringe dipped inside the reactor. Care was taken to ensure that the samples were taken close enough to the impeller of the stirrer for each experiment to ensure comparability of results. The particle size distribution of these samples were analyzed using the Zetasizer 2000 (λ = 633 nm) from the Malvern Company based on the principle of dynamic light scattering. Measurements are performed at a scattering angle of 90° and 25°. The first samples are taken after 5 hours into the experiment as samples taken before this time had size distributions in the micro range. This was revealed by analysis from the Zetasizer (from the Malvern Company) which measures size distributions in the micro range.

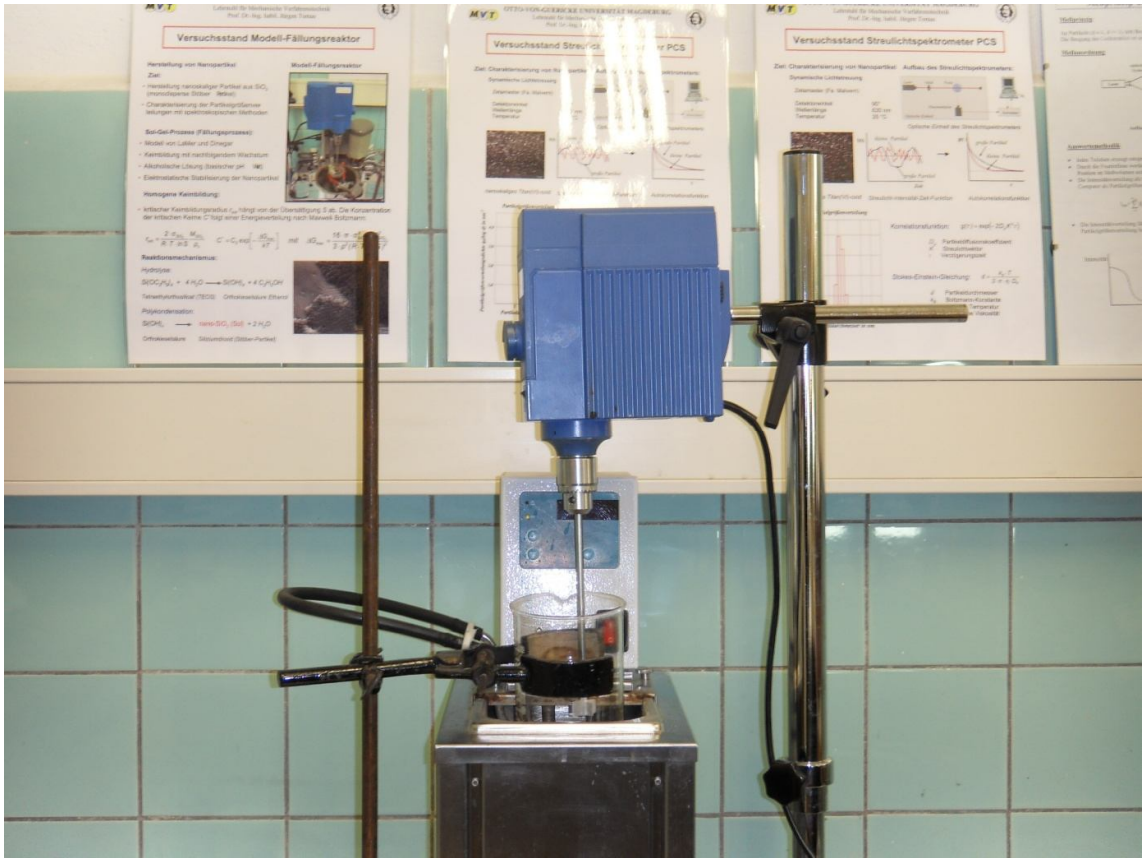

Fig 5.1: Experimental Set-up

5.2 Variation in Process Parameters

Since the objective of the study includes an investigation of the influence of process parameters on the synthesis of Titanium (IV)-oxide nanoparticles and the prospects of up-scaling of the process to industrial scale, the experiment involved a variation in the impeller geometry and in the shear rate of the stirrers employed. The volumes of the precursor and dispersant were also varied proportionately for each case. This is reviewed below.

5.2.1 Variation of Shear rate

The shear rate of the stirrer was varied to investigate the influence of an increased shear on the kinetics of the synthesis of Titanium (IV)-oxide nanoparticles. A motor with a variable speed control was connected to the stirrer to enable speed variation to be achieved. Experiments were carried out at shear rates of $\dot{\gamma}$ = 370 and 960 s^{-1} corresponding to stirrer rotational speeds of 500 rpm and 1000 rpm respectively for solvent (nitric acid) volumes up to 1 litre. For higher volumes, the experiments were only conducted at a shear rate of 370 s^{-1} as increased shear resulted in severe agitation and vibrations raising concerns about safety.

5.2.2 Variation of Stirrer geometry

The influence of the geometry of stirrer on the kinetics of the synthesis of Titanium (IV)-oxide nanoparticles was also considered. Two types of stirrers were used – the pitched blade and the crossed blade (shown in fig. 5.2 below) stirrers were employed. The impeller acts as an agitator, creating a flow pattern, enabling the liquid medium to circulate through the vessel and eventually return to the impeller [26]. A 3-blade pitched impeller and a 4- blade crossed impeller were used and for larger volumes, a bigger crossed blade impeller was also used.

The type of impeller used and the number of blades are design choices which affect the circulation rate of the liquid, the velocity patterns and the power consumed. Typically, the number of impeller blades range between 4 to 16 and special situation such as the depth of the agitator in the reactor or the reactor depth may be critical to achieving desired result [26].

The pitched impeller is generally recommended for applications which require an average or high speed where mixing tasks with medium or high viscosity. It offers excellent mixing properties for homogenization and suspensions. These models create an axial flow. In contrast, the crossed blade is used in applications which require an average speed or when mixing tasks with little or average viscosity.

5.2.3 Homogenization Time

Particle sizes were measured on an hourly basis from 5 hours into the experiment. Sol homogenization for Titanium (IV)-oxide was achieved after 5 hours as samples taken earlier than this revealed size distributions that had not transited into the nano range hence could not considered. This was also reported by [77].

5.3 Up-scaling

In investigating the prospects for scaling-up the synthesis process from the laboratory scale to the industrial scale, the volumes of the solvent and dispersant were increased in successions according to a constant ratio. Experiments were run for 24 hours for volumes up to 1000 ml while experiments for larger volumes were run between 9 to 10 hours due to safety concerns.

5.4 The Freeze Drying Technique

The long-term stability of nanoparticles in suspensions, as compared to the dry formulations, is poor due to the large surface area and high surface energy [78]. The poor stability in an aqueous medium of these systems forms a real barrier against the application of nanoparticles

for clinical purposes. Freeze-drying has been considered as a good technique to improve the long-term stability of colloidal nanoparticles hence this method has been used to isolate the TiO_2 nanoparticles from the suspension.

The freeze-drying process is based on the fast freezing of an aqueous salt solution containing the desired cation or cations and the subsequent sublimation of ice under vacuum conditions. Freezing should be accomplished as quickly as possible, to preserve the solution homogeneity. The most common method involves the spraying of the solution into liquid nitrogen, thus being highly efficient. However, other refrigerant systems as hexane cooled with an acetone-ice mixture have been studied [79, 81]. As a result, porous spherical granules of the anhydrous salt with a high surface area are obtained. A conventional thermal treatment is later required in order to remove the anion and to grow the oxide nanoparticles [79,80,81].

CHAPTER 6

DISCUSSION OF EXPERIMENTAL AND MODELING RESULTS

The objective of the present work is to investigate the kinetics the disintegration process during the sol-gel synthesis of Titanium (IV)-oxide nanoparticles. As stated in the previous chapter, the Zetasizer (from the Malvern company) was used to sample analysis after 5 hours experiment run.

The dynamic evolution of the particle size distribution (PSD) can be represented as a cumulative distribution $Q_0(d)$ or as a particle size frequency distribution $q_0(d)$. Presenting the evolution of PSD in terms of cumulative distribution enables a clear visualization of the increase or reduction of particle size with time as evidenced by the shift of the size distribution curve to the right or the left. In contrast, the particle size frequency distribution curve does not provide this option as what is seen is only the total number of particles present.

Since the desired product properties might vary with particle size as well as with the degree of aggregation or the aggregate structure, controlling of the PSD and the aggregate structure is a key criterion for product quality. New and improved products can then be designed by adjusting and optimizing the PSD and the particle structure.

In the next sections, the influence of each parameter considered on the overall kinetics of the disintegration process will be discussed. An overview of the experimental results is presented and later a comparison is also drawn between experimental and simulation results. Two redispersion or brakeage kernels (Austin and Diemer kernels) and an agglomeration kernel (constant kernel) have been used in validating the experimental results. A single agglomeration kernel is used as experimental results suggest that redispersion was the dominant mechanism over the time of the experiment. For uniformity, the experimental and simulation results studied has been limited to the first nine hours of the experiment. The simulation was run on MATLAB software provided by the MathWorks Company.

6.1 Experimental Results – An Overview

A general overview of the experimental results is presented in this section. For the various experiments conducted, the ratio of precursor and dispersant used is kept constant while other process parameters – the shear rate, stirrer geometry and total reaction volume – are varied. The overall influence of these parameters on the kinetics of the disintegration process and evolution of the particle size distribution are also investigated.

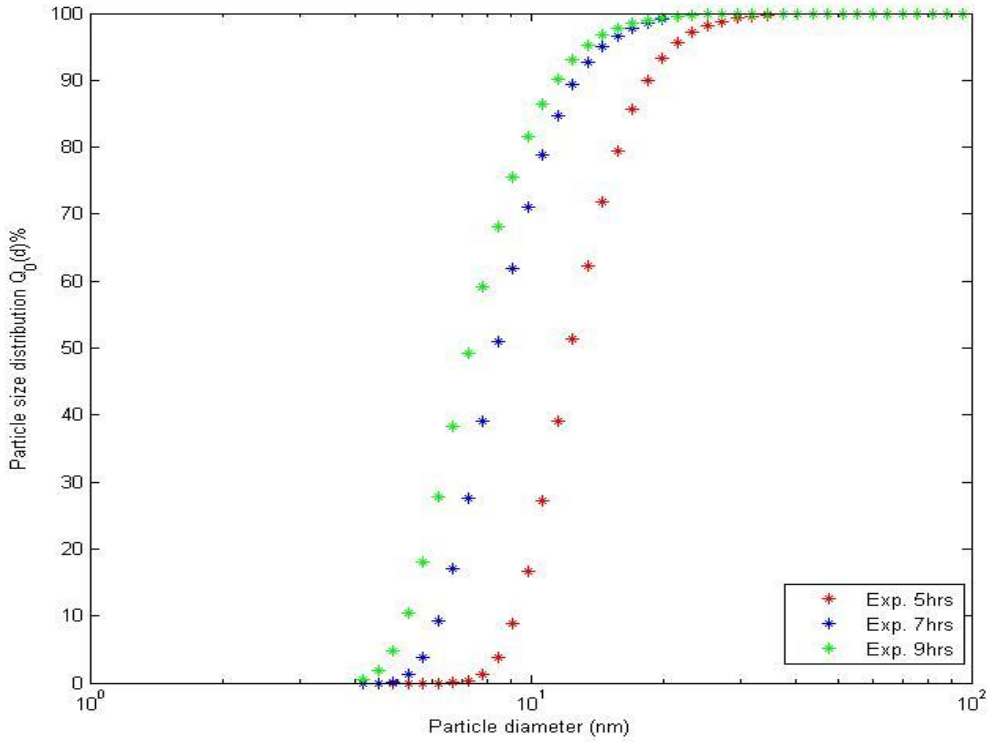

Fig. 6.1: Dynamics of the evolution of Particle size distribution $Q_0(d)$ during the experimental sol–gel TiO_2 nanoparticles process at $\dot{\gamma} = 370\ s^{-1}$, reaction volume of 600 ml and a precursor – dispersant ratio of 1:14.

The dynamics of the evolution of particle size distribution $Q_0(d)$ is explained by Fig. 6.1 for a reaction volume of 600 ml. It is obvious that the reaction time plays an influence on the synthesis of Titanium (IV) – oxide. A general decrease in the trend of particle size as homogenization progresses from the beginning to the end of the synthesis period is noted. The resulting decrease in particle size is a result of the redispersion process that dominates the larger part of the synthesis period. The particles split into smaller fragments leading to a significant increase in the number of particles while the total mass of the system is conserved.

A similar observation is noted when the reaction volume is increased and the when the shear rate is altered. In all these cases, the precursor-dispersant ratio is held constant at a ratio of 1: 14. Figs. 6.2 and 6.3 below depict these cases:

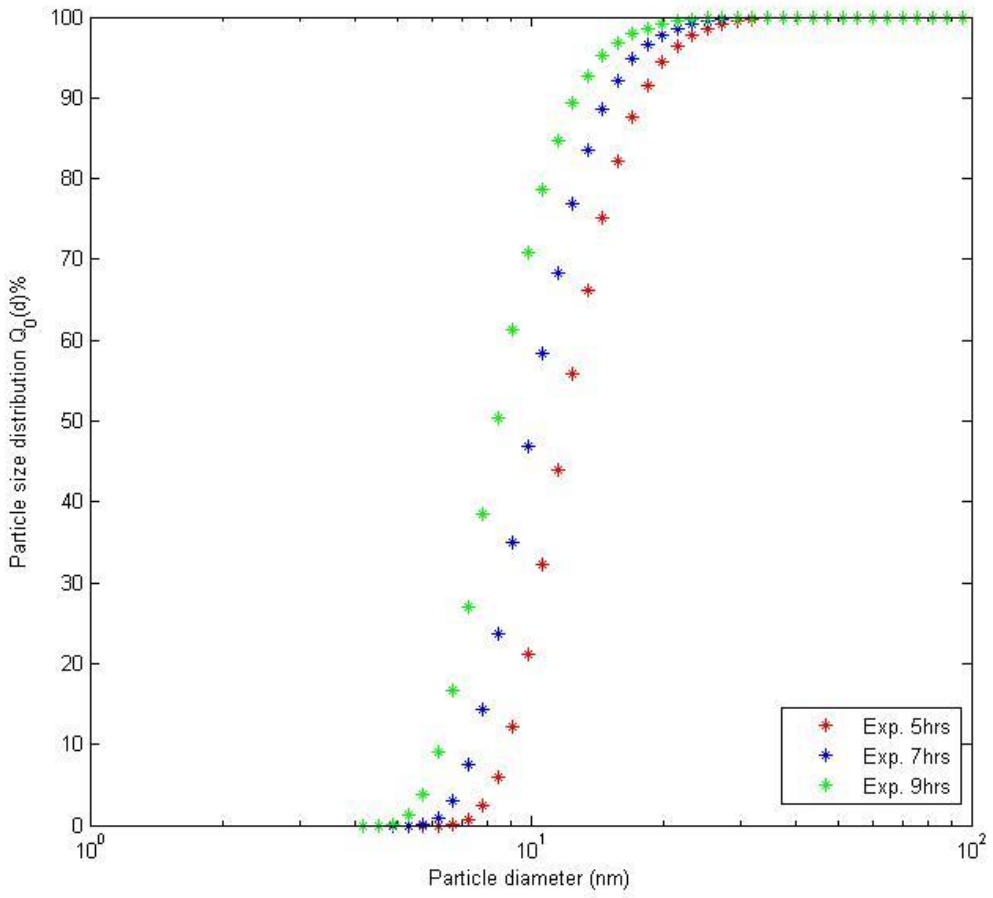

Fig. 6.2: Dynamics of the evolution of Particle size distribution $Q_0(d)$ during the experimental sol–gel TiO_2 nanoparticles process at $\dot{\gamma}$ = 370 s^{-1}, reaction volume of 1070 ml and a precursor – dispersant ratio of 1:14.

As seen in Fig. 6.2 above, an increase in the reaction volume while other process conditions are held constant results in a decrease in the particle size as homogenization progresses from 5 h to 9 h. The result obtained when the reaction volume is increased is comparable with that obtained for smaller volumes. This suggests that the manner in which the particle size distribution evolves is not influenced by the reaction volume when other factors are held constant.

The influence of an increased shear is also observed in Fig. 6.3 below.

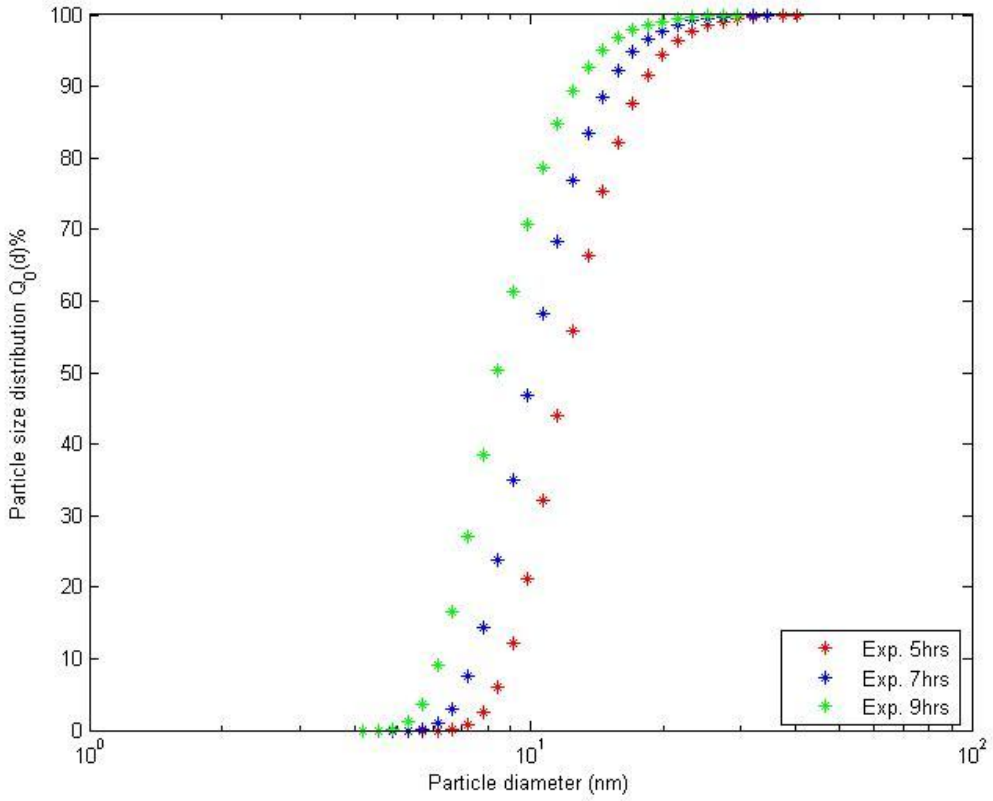

Fig. 6.3: Dynamics of the evolution of Particle size distribution $Q_0(d)$ during the experimental sol–gel TiO_2 nanoparticles process at $\dot{\gamma}$ = 960 s^{-1}, reaction volume of 1070 ml and a precursor – dispersant ratio of 1:14.

The shear rate was varied to investigate the influence of changes in the hydrodynamic conditions of the process on the particle size distribution and particle structure during reaction. It can be seen from Fig. 6.3 above that the effect of a higher shear rate on the kinetics of the evolution of the particle size distribution is not very pronounced when compared with the result obtained produced in Fig 6.2 when a shear rate of $\dot{\gamma}$ = 370 s^{-1} was used. However, it is known that higher shear rates generally produce lower particle sizes [85]. The influence of shear rates will be discussed more extensively in the next sections.

6.2 Simulation Results

In this section, the simulation results are compared with experimental results. We also present the influence of process parameters on the overall kinetics of the disintegration process in this section.

6.2.1 Influence of Process Parameters on PSD

The influence of some process parameters on the evolution of PSD are considered below:

6.2.1.1 Influence of Shear rate on the PSD

In investigating the influence of shear rate on the evolution of the particle size distribution, the experimental and numerical results obtained during the synthesis of Titanium (IV)-oxide nanoparticles using a total reaction volume of 600 ml is considered. The synthesis was conducted at $\dot{\gamma} = 370\ s^{-1}$ and $\dot{\gamma} = 960\ s^{-1}$ respectively. The experimental results were compared with numerical solutions using a combination of two breakage kernels – the Austin and Diemer kernel – and the constant agglomeration kernel.

In general, for the Austin kernel, the following parameters are used viz: $\gamma = 10, \emptyset = 0.1;\ \beta = 4;\ \mu = 0.4$. Values of $p = 2; c = 11$ was also used for the Diemer kernel.

$\gamma, \emptyset, \beta$ and μ are dimensionless material constants, p describes the number of fragments per disintegration event and c determines the shape of the daughter distribution.

Also, the 5 hrs experimental result has been taken as the initial condition in all cases. Comparisons are made between particle size distributions at various time intervals during the course of the experiment.

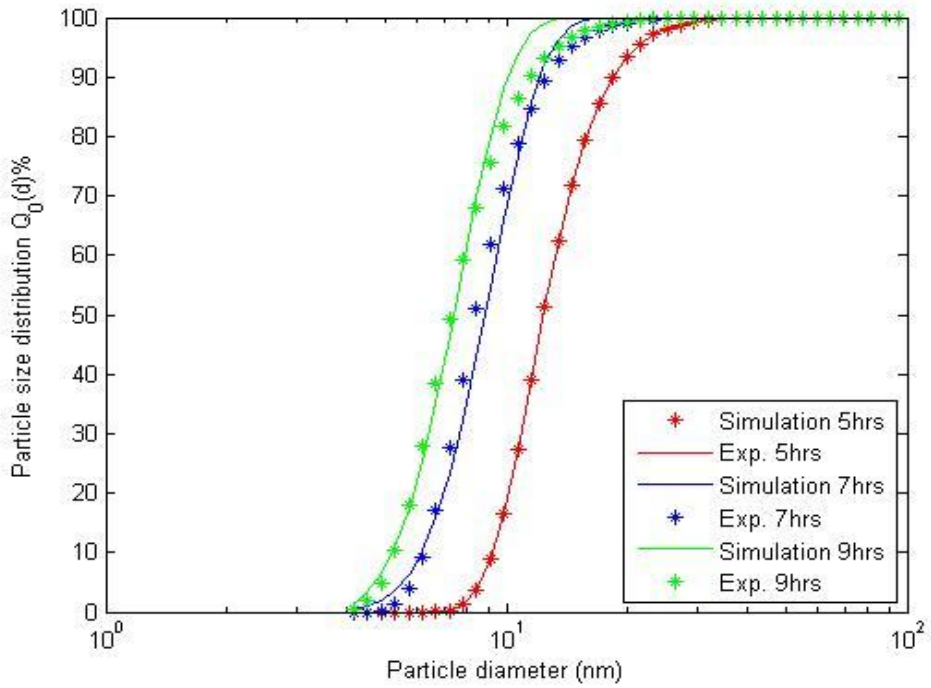

Fig. 6.4: Particle size distribution $Q_0(d)$ providing a comparison between experimental data of the sol–gel TiO_2 nanoparticles process at $\dot{\gamma} = 370\ s^{-1}$, reaction volume of 600ml and a precursor – dispersant ratio of 1:14. The simulated evolution of PSD was depicted by the Austin kernel.

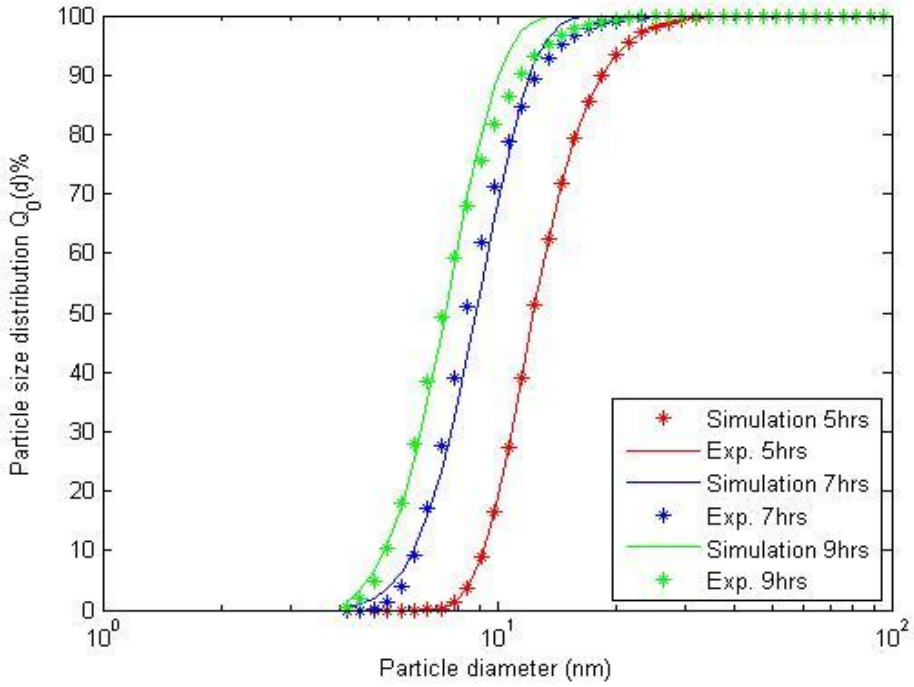

Fig. 6.5: Particle size distribution $Q_0(d)$ providing a comparison between experimental data of the sol–gel TiO_2 nanoparticles process at $\dot{\gamma}$ = 370 s^{-1}, reaction volume of 600ml and a precursor – dispersant ratio of 1:14. The simulated evolution of PSD is depicted by the Diemer kernel.

Figs. 6.4 and 6.5 above shows results obtained from comparisons between experimental and simulation results by using the Austin and Diemer Kernel when TiO_2 nanoparticles synthesis takes place with a total reaction volume of 600 ml. As evident from the results above, the simulation results depicted by the Austin and Diemer kernels show profound agreement with the experimental results. A general decrease in particle size as homogenization time increases as the synthesis progressed from 5 hours to 9 hours is noted. The bigger particles observed during the early stages of the experiment are due to the agglomeration of the primary particles. The agglomeration process is due to the rapid collision and bonding of the particles. As the experiment progressed, redispersion sets in and the particle size distribution evolves rapidly. Particle size began to distribute into wide variety of ranges and this progresses until a steady state is achieved.

The implication of this is that agglomeration plays a larger role during the early stage of the experiment and breakage sets in as the experiment progressed. It is also noted from the nature of the curves obtained the particles obtained are monodispersed in nature.

An increase in the shear rate from $\dot{\gamma}$ = 370 s^{-1} to $\dot{\gamma}$ = 960 $s^{-1}$for the same ratio of precursor and dispersant had no significant effect on the evolution of the particle size distribution. This is depicted in figs. 6.6 and 6.7 below:

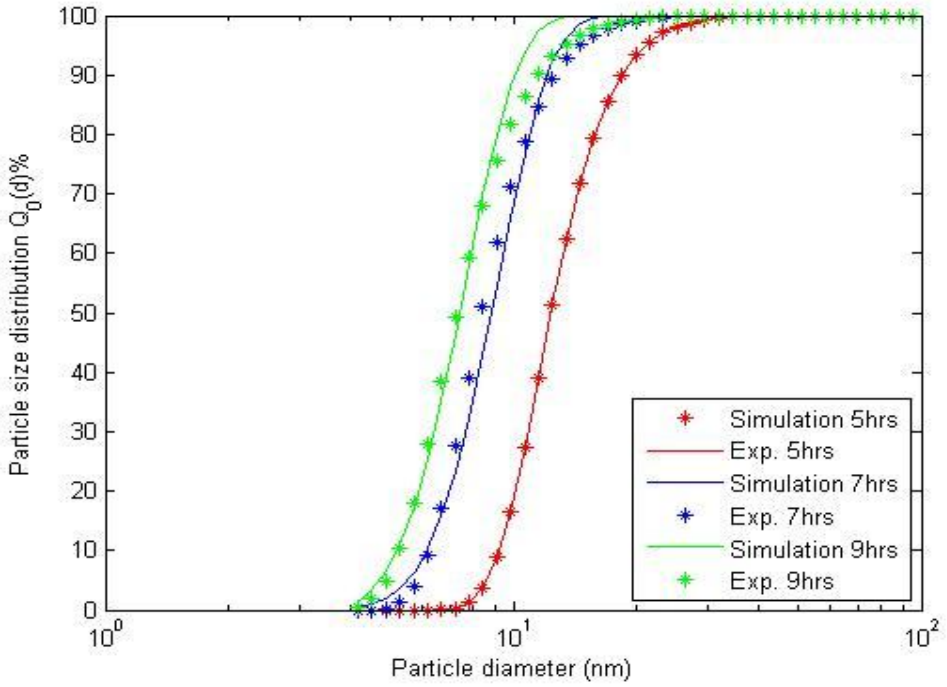

Fig. 6.6: Particle size distribution $Q_0(d)$ providing a comparison between experimental data of the TiO_2 nanoparticles process at $\dot{\gamma}$ = 960 s^{-1} , reaction volume of 600ml and a precursor – dispersant ratio of 1:14. The simulated evolution of PSD was depicted by the Austin kernel.

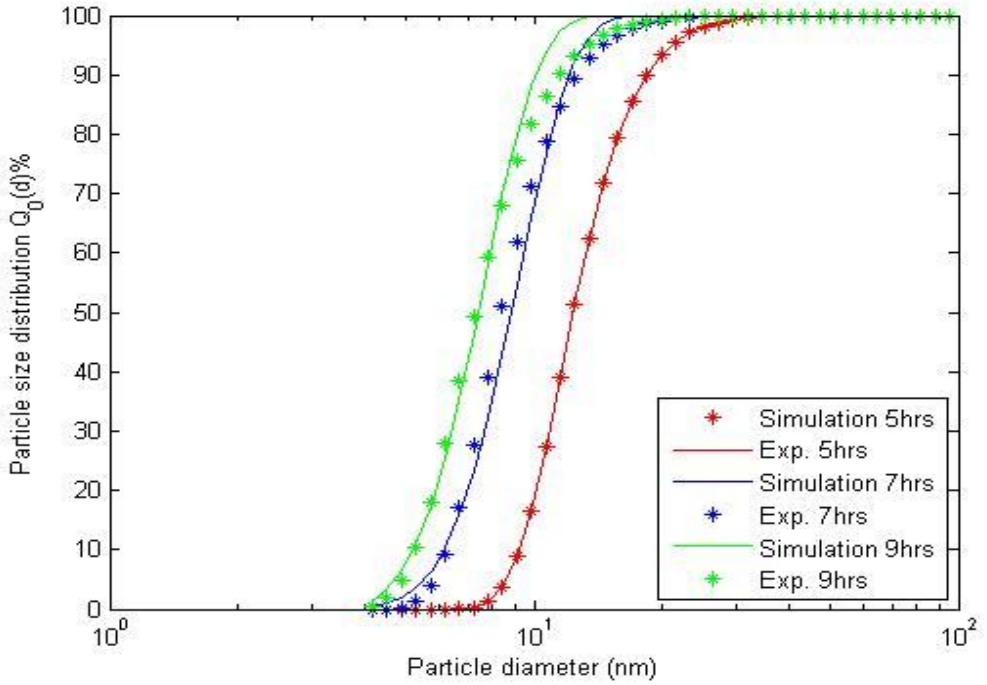

Fig. 6.7: Particle size distribution $Q_0(d)$ providing a comparison between experimental data of the TiO_2 nanoparticles process at $\dot{\gamma}$ = 960 s^{-1}, reaction volume of 600ml and a precursor – dispersant ratio of 1:14. The simulated evolution of PSD was depicted by the Diemer kernel.

As seen in figs. 6.6 and 6.7 above, an increased shear has little or no influence on the evolution of size distribution for both disintegration kernels. This is consistent with results obtained in [82] where the influence of the hydrodynamics at higher increased shear rates related to TiO_2 nanoparticles agglomeration and disintegration were investigated. It was reported that the formation of nano-scaled particles is much less influenced by applied shear rates of conventional blade stirrers.

The results obtained at $\dot{\gamma}$ = 370 and 960 s^{-1} are similar with a decrease in size distribution as homogenization time increases. This suggests that redispersion or the breakage process is the dominant mechanism in the synthesis of TiO_2 nanoparticles.

6.2.1.2 Influence of Stirrer Geometry on the PSD

In investigating the influence of stirrer geometry on the evolution of PSD, experiments were conducted with stirrers with pitched blade and crossed blade impellers. The stirrers serve to provide good mixing and homogeneity of the dispersant-precursor solution.

A comparison between experimental and a simulation result for the two disintegration kernels when the crossed blade stirrer is used is shown in figs. 6.8 and 6.9 below for total reaction volume of 2140 ml is shown below:

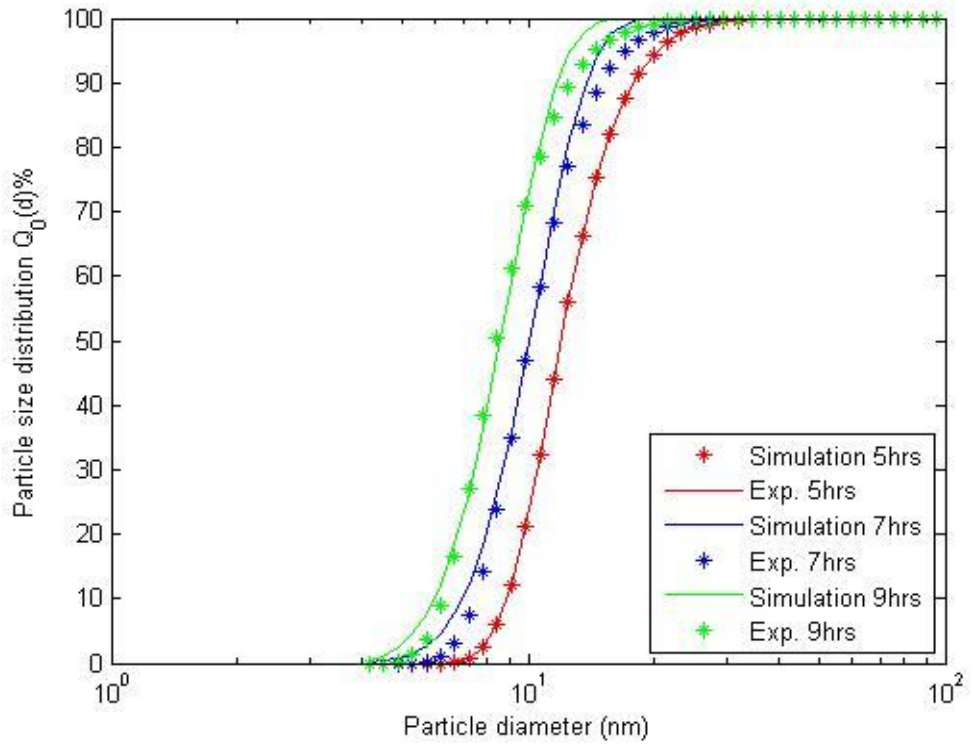

Fig. 6.8: Particle size distribution $Q_0(d)$ providing a comparison between experimental data of the TiO_2 nanoparticles process for a reaction volume of 2140ml and precursor – dispersant ratio of 1:14 when a stirrer with a crossed blade impeller is used. The simulated evolution of PSD was depicted by the Austin kernel.

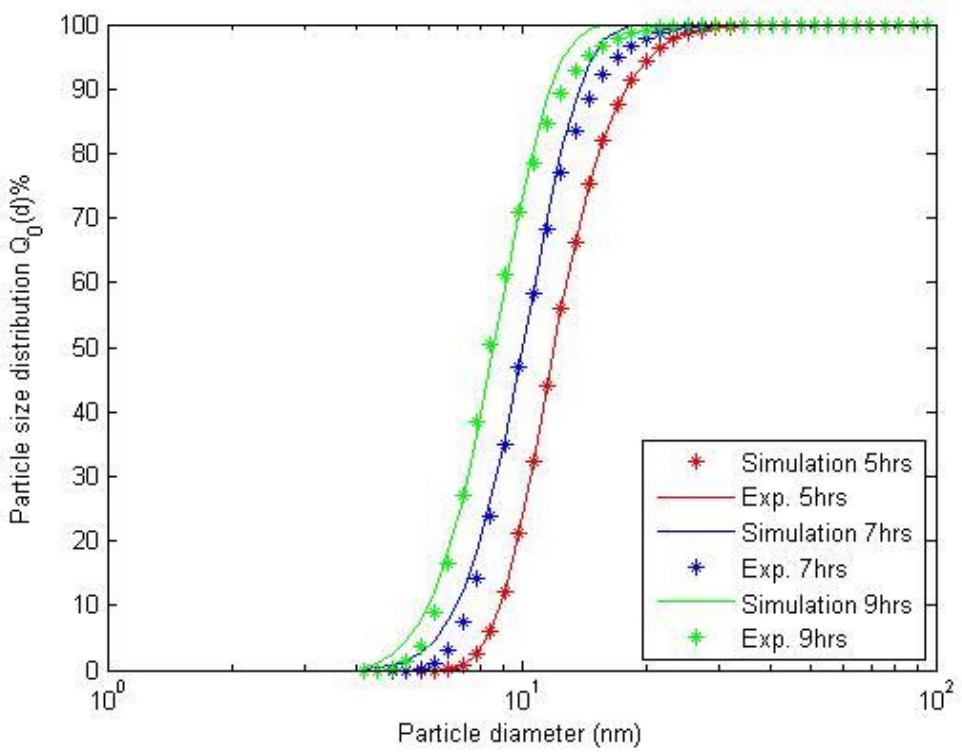

Fig. 6. 9: Particle size distribution $Q_0(d)$ providing a comparison between experimental data of the TiO_2 nanoparticles process for a reaction volume of 2140ml and precursor – dispersant ratio of 1: 14 when a stirrer with a crossed blade impeller is used. The simulated evolution of PSD was depicted by the Diemer kernel.

As seen above, the results obtained for the Austin and Diemer kernels are identical when the crossed blade stirrer is used. Redispersion dominates while average particle diameter is in the order of 8-10 nm. This suggests that the geometry of the stirrer does not influence the kinetics of the disintegration process. This observation is corroborated by observing the dynamics of the synthesis when the pitched blade stirrer is employed to stimulate the hydrodynamics of the disintegration process for the same volume and concentration of dispersant and precursor as seen in figs. 6.10 and 6.11 below. As in the previous cases, the Austin and Diemer kernels are considered.

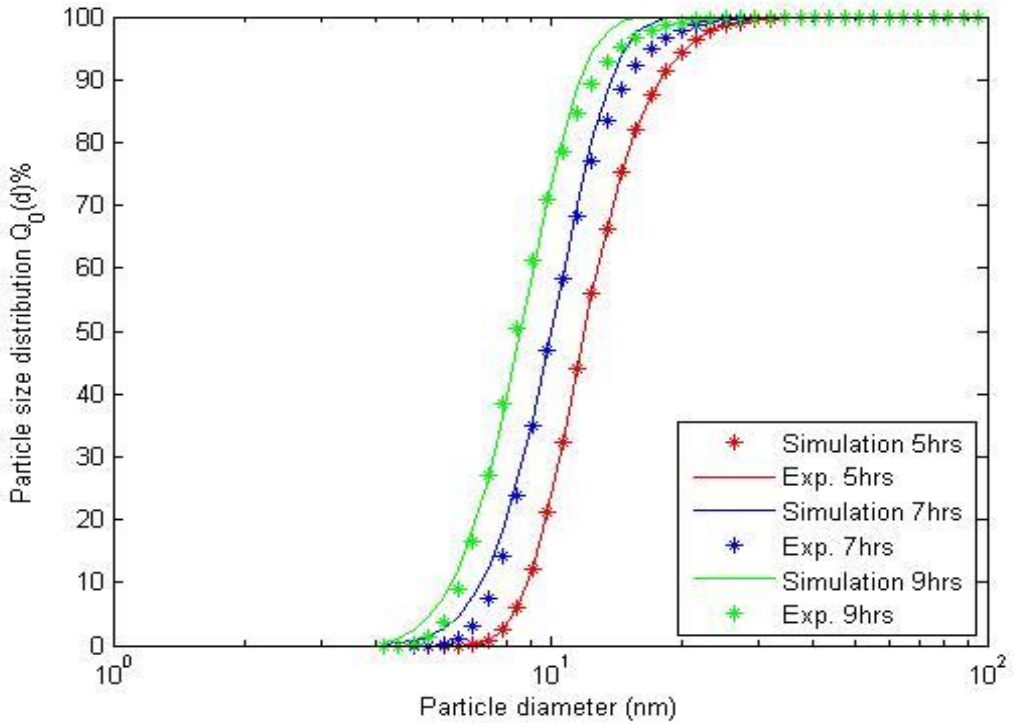

Fig. 6. 10: Particle size distribution $Q_0(d)$ providing a comparison between experimental data of the TiO_2 nanoparticles process for a reaction volume of 2140ml and precursor – dispersant ratio of 1:14 when a stirrer with a pitched blade impeller is used. The simulated evolution of PSD was depicted by the Austin kernel.

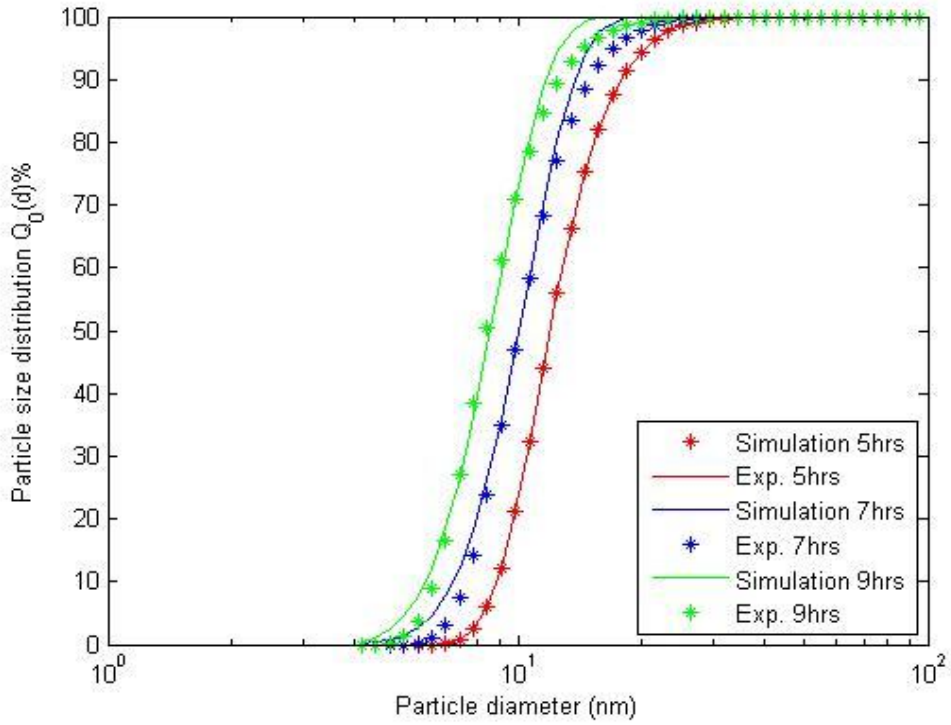

Fig. 6. 11: Particle size distribution $Q_0(d)$ providing a comparison between experimental data of the TiO_2 nanoparticles process for a reaction volume of 2140ml and a precursor – dispersant ratio of 1:14 when a stirrer with a pitched blade impeller is used. The simulated evolution of PSD was depicted by the Diemer kernel.

Figs. 6.10 and 6.11 show the comparisons between the experimental and the simulation results by using the Austin and Diemer kernels respectively for a disintegration process where stirrer with a pitched blade impeller is used. The results reveal excellent agreement between experimental and simulation results for both kernels suggesting that the two disintegration kernels give an accurate prediction of the experimental results. This is revealed by the almost perfect match obtained between the size distribution curves for the time intervals considered. In comparison, the results agree well with the cases in Fig. 6.8 and 6.9 where a stirrer with a crossed blade impeller is employed.

The implication of the above findings is that the role played by the stirrer geometry is not significant in defining the overall process kinetics.

6.2.1.3 Homogenization time

For all the cases considered, it is evident that the reaction time plays a significant role in the synthesis of Titanium (IV)-oxide nanoparticles. Experimental and simulation results revealed that an increase in homogenization time (in our case, a synthesis period from 5 h to 9 h) leads a corresponding decrease in size distribution of Titanium (IV)-oxide nanoparticles as shown in Figs. 6.4 to 6.11 above.

Monodispersed particles were obtained for homogenization times between 5 h to 9h. This differs from the findings of [84] in which monodispersed Titanium (IV)-oxide particles were after a reaction period of 10 h. This could be attributed to nature of the surfactants (polyethylene glycol and ethylene glycol) used in the synthesis.

6.2.1.4 Upscaling

The process was scaled up in a stepwise manner by maintaining the precursor –dispersant ratio of 1 : 14 up to a total reaction volume of 3210 ml to investigate the prospect available for the industrial synthesis of Titanium (IV)-oxide nanoparticles based on the experimental conditions considered in this work. A proportionate increase in the reaction volume did not significantly alter the kinetics of the disintegration process. This suggests a positive prospect for implementing the synthesis on an industrial case based on the conditions considered in this work.

However, concerns about safety may necessitate more innovative design of the process.

6.3 Particle Morphology

The morphology of the particles were visualised by transmission electron microscopy. This is shown in fig. 6.9 (a-d) below.

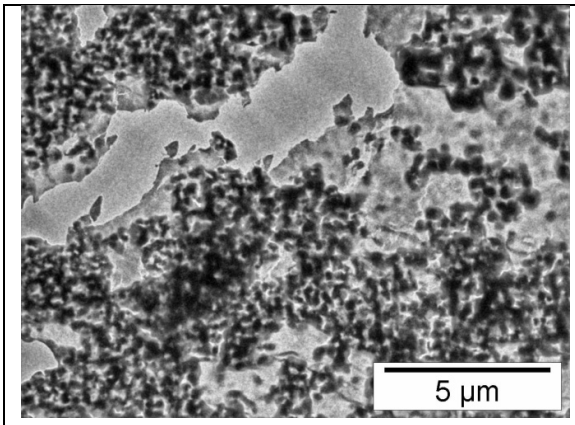

(a) TiO_2, HNO_3 TEM - Picture show the morphology of TiO_2 particles - connected in fractals and build agglomerates with a size about 200 nm

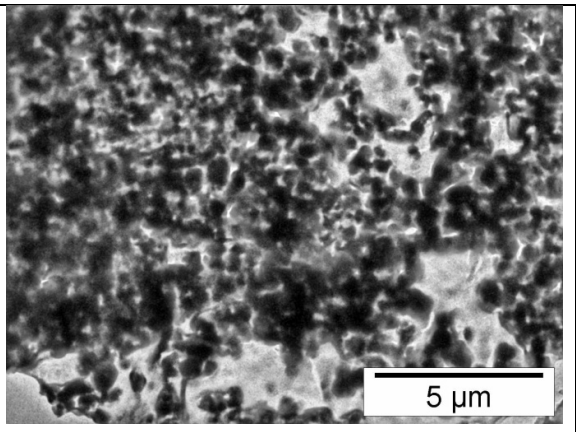

(b)TiO_2, HNO_3 TEM - This shows the morphology of TiO_2 particles - connected in fractals and build agglomerates with a size about 200 nm

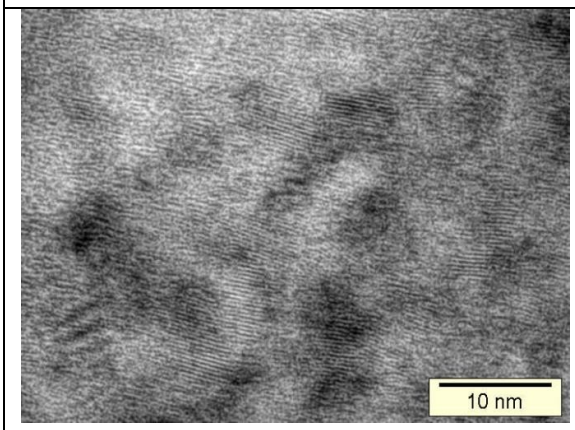

(c)TiO_2, HNO_3 HRTEM – Crystal structures is also confirmed by high resolution TEM

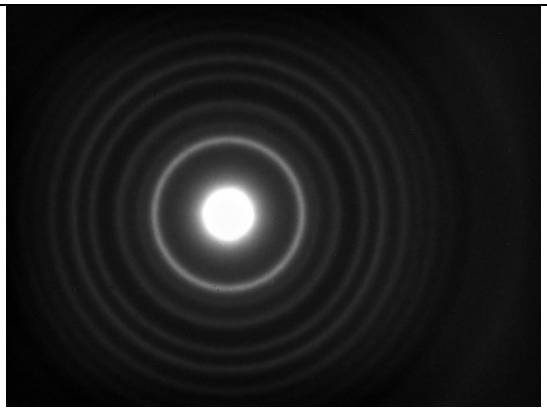

(d)TiO_2, HNO_3 TEM –diffraction image shows that these nanoparticles have a crystal structure

Fig 6.12: Enlarged TEM images of TiO_2 nanoparticles with 0.1M HNO_3 as dispersant and at T= 50°C.

The TEM visualizations shown in fig 6.9 (a) and (b) above reveal the build-up of the Titanium (IV)-oxide nanoparticles agglomerates with a size of 200 nm from a connection of fractals. High resolution and Diffraction images shown in figs. 6.9 (c) and (d) confirm the crystalline structure of Titanium (IV)-oxide nanoparticles. This enhances its application in a wide range of industrial applications.

6.4 Zeta Potential and Specific Surface Area Measurements

Electrophoretic mobility measurements were obtained by using the Zetasizer Nano (Malvern Instruments Inc.) and reproducibility was verified by performing repeated measurements for all experimental samples.

The Zeta potential measurements gave values within the range of 33.3mV and 41mV. These values are in agreement with the general rule of thumb of zeta potential values greater than +30 mV or lower than –30 mV for ensuring electrostatic stability of particle formulations [83].

The specific surface area was also measured for the sample using the BET method. A specific surface area value of 120m^2/g was obtained.

CHAPTER 7

CONCLUSIONS AND SUGGESTIONS FOR FUTURE WORK

This kinetics of the disintegration process during the synthesis of Titanium (IV) oxide nanoparticles via the sol-gel technique has been studied in this work. The influences of certain process parameters on the dynamic evolution of the particle size distributions have also been considered. Parameters studied include the influence of shear rate, stirrer geometry and a proportionate increase in the reaction volume.

7.1 Conclusions

1. During the sol-gel synthesis of Titanium (IV)-oxide nanoparticles using Titanium tetraisopropoxide (TTIP) as precursor and Nitric acid as dispersant, transition to the nano-range takes place after 5 hours of experimental run.
2. Redispersion is the dominant mechanism during the sol-gel synthesis of Titanium (IV)-oxide nanoparticles. This is evidenced by successive reduction in particle size distribution of the formed nanoparticles as experiment progressed until sol homogenization is achieved.
3. An increased shear rate from at $\dot{\gamma} = 370\ s^{-1}$ to $\dot{\gamma} = 960\ s^{-1}$ has little or no effect on the kinetics of the disintegration process and the evolution of size distribution when other experimental conditions are held constant. This is corroborated by identical experimental and simulation results obtained when the Austin and Diemer kernels are employed to describe the disintegration process.
4. The effect of a change in the geometry of the impeller of the stirrers employed (pitched blade and crossed blade) on the dynamic evolution of particle size distribution is not noticeable based on the experimental and simulation results obtained. The results obtained for the Austin and Diemer kernels were comparable for the two cases considered.
5. Results obtained reveal strong prospects for up scaling the process from laboratory to industrial scale. A proportionate increase in the volume of dispersant and precursor used did not significantly impact on the evolution of the size distribution. The simulation results also show good agreement with experimental results in this case.
6. The stability of the nanoparticles formed is confirmed by the values obtained from electrophoretic mobility measurements for all experimental cases considered. The Zeta potential measurements gave values within the range of +33.3mV and +41mV.

7. The crystalline nature of Titanium (IV)-oxide nanoparticles formed is confirmed by high resolution TEM images obtained.
8. Isolation of the particles was possible via the freeze drying technique and a specific surface area value of 120m^2/g was obtained for the 3 litre sample via the BET method.

7.2 Suggestions for future work

This research provides an opportunity to explore more possibilities in the synthesis of Titanium (IV)-oxide nanoparticles for more conclusive results to be obtained.

1. An increase in the size of the impeller blade as the volume of the dispersant-precursor mixture increases could provide more insights to the effect of stirrer geometry on the kinetics of the disintegration process.
2. The validity of the experimental results could be further verified by numerical simulations based on other ordinary differential equation solving techniques and the use of the shear breakage kernel. Models that capture longer hours of experimental run could also be helpful.

References

[1] Parida, K. M., Sahu N., Biswal N. R., Naik, and A. C. Pradhan, "Preparation, characterization, and photocatalytic activity of sulfate-modified Titanium (IV)-oxide for degradation of methyl orange under visible light," *Journal of Colloid and Interface Science*, Vol. 318, No. 2, (2008) pp. 231–237.

[2] Rashed, M. N., El-Amin, A. A. "Photocatalytic degradation of methyl orange in aqueous TiO_2 under different solar irradiation sources," *International Journal of Physical Sciences*, vol. 2, no. 3, (2007) pp. 73–81.

[3] Prieto, O., Fermoso, J., Irusta, R. "Photocatalytic degradation of toluene in air using a fluidized bed photoreactor," *International Journal of Photoenergy*, vol. 2007, Article ID 32859, (2007).

[4] Su, W., Chen, J., Wu, L. , Wang, X., Fu, X. "Visible light photocatalysis on praseodymium(III)-nitrate-modified TiO_2 prepared by an ultrasound method," *Applied Catalysis B*, vol. 77, no. 3-4, (2008) pp. 264–271.

[5] Hafizah, N., Sopyan, I. Nanosized TiO_2 Photocatalyst Powder via Sol-GelMethod: Effect of Hydrolysis Degree on Powder Properties. *Int. J. Photoenergy*. Volume 2009, Article ID 962783.

[6] William M. Yen, Shigeo Shionoya, Hajime Yamamoto. *Phosphor handbook*, pp. 382 – 385

[7] Robert J. Hunter. Introduction to modern colloid science, *Oxford University press Inc*, New York (1999).

[8] M. Sadat-Shojai. *J. Iran. Chem. Soc*., Vol. 6, No. 2, June 2009, pp. 386-392.

[9] Rumpf, H. Particle Technology: Powder Technology Series, *Chapman and Hall*, London (1990)

[10] Ferraz, M.P., Monteiro, F.J., Manuel, C.M., *J. Appl. Biomater. Biomech*. 2 (2004) 74.

[11] Vazquez, C.G., Barba, C.P., Munguia, N., *Rev. Mex. Fis.* 51 (2005) 284.

[12] Cho, J.S., Kang, Y.C., *J. Alloy. Compd.* 464 (2008) 282.

[13] K. Lin, J. Chang, R. Cheng, M. Ruan, Mater. Lett. 61 (2007) 1683

[14] Jeffrey Brinker C., et al. Sol-gel science: the physics and chemistry of sol-gel processing (1990) pp. 839-840.

[15] Bradley, D. C.; Mehrotra, R.; Rothwell, I.; Singh, A. "Alkoxo and Aryloxo Derivatives of Metals" *Academic Press, San Diego*, (2001).

[16] Tatsul Sato and Richard Ruch, Stabilization of colloidal dispersion by polymer adsorption. *Marcel Dekker Inc., New York*, (1980).

[17] Jingyu S. *Steric Stabilization, Group Inorganic Material Science, Ohio* C.I.S.M (2002).

[18] Somasundaran P. Encyclopedia of surface and colloid science. Vol 2. pp. 6048 – 50.

[19] Zeta Potential: A complete course in 5 minutes. *Zeta Master Inc.* USA (2000)

[20] Mandzy N. et al., Powder Technology 160 (2005) 121–126.

[21] Tatsul Sato, Richard Ruch, Stabilization of colloidal dispersion by polymer adsorption. Marcel Dekker Inc., (1980) New York.

[22] Napper, D.H. Polymeric Stabilization of Colloidal Dispersions. *Academic Press, London*, (1983).

[23] Ginzberg B., Bilmes, S.A., *Progr. Colloid Polym. Sci* 102, 51 (1996).

[24] Vorkapic, D., and Matsoukas, T., Effect of temperature and alcohols in the preparation of Titanium (IV)-oxide nanoparticles from alkoxides (1998)

[25] Cordero-cabrera, M.C., et.al, Effect of processing parameters on the particle size and stabilisation of Titanium (IV)-oxide sols *J. of Mat. Sci.* 40 (2005) 3709 – 3714

[26] Mc Cabe, W. L., Smith, J. C., Harriot, P., Unit operations of Chemical Engineering, 6th Edition, *McGraw-Hill, New York* (2001).

[27] James B., et al., Surface application of paper *chemicals* pp. 122-123 (1997)

[28] Hintz, W., Aman, S., Tomas, J. Nanoparticle Technology, Lecture material, Otto-von-Guericke University, Magdeburg (2004)

[29] Derjaguin, B.V., and Landau, L. (1941) Acta Physiochim. URSS, 14, 633.

[30] Measuring Zeta Potential: A New Technique, Technical Note from the Malvern Company.

[31] Measuring Zeta Potential: Laser Doppler Electrophoresis, Technical Note from the Malvern Company

[32] Christopher R., et al. The effects of processing on the morphology of nanoparticles. *Mat. Res. Soc.(2004)*

[33] Bushell, G. C., Yan, T.D., Woodfield, D., Raper, J., Amal, R., On techniques for the measurement of mass fractal dimension of agglomerates. *Adv. In colloid and interface science*, 95, (2002), pp. 1-50.

[34] Barreteau, C., *et al., Eur. Phys. J. D* 11 (2000) 395.

[35] Perrey, C.R., *et al, Microsc. Microanal.* 10 Suppl.2 (2004) 55.

[36] Henry, C., Size Effects on Structure and Morphology of Free or Supported Nanoparticles, Springer Berlin Heidelberg (2008).

[37] Fagerlund G., Determination of specific surface by the BET method, *Mat. and Structures*, (2006), pp. 239-245.

[38] BAM Reference Procedure; Precision Measurement of the Specific Surface Area of Solids by Gas Adsorption, Microprobing and Microstructure Analysis (2005).

[39] Brunauer, Emmet, Teller, *Journal of the American Chemical Society*, Vol. 60, 1938, p 309.

[40] Kumar, J., Numerical approximations of population balance equations in particulate systems, PhD Dissertation, *Fakultät für Mathematik, Otto-von-Guericke Universität* (2006).

[41] Gerstlaur, A., *Herleitung und Reduction populationsdynamischer Modelle am Beispiel der Flüssig-Flüssig-Extraction.* PhD thesis, University of Stuttgart, Germany, (1999).

[42] Ramamoorthy, V. *Redispersion kinetics during the sol-gel synthesis of titanium dioxide nanoparticles: Experimental approach and computer aided simulation.* M.Sc thesis, *Faculty of process and systems Engineering, Otto-von-Guericke Universität* (2005).

[43] Park, S. H., Rogak, S. H., A novel fixed sectional model for the formation and growth of aerosol agglomerates. *Aerosol Science,* 35, (2004), pp.3681-3698.

[44] Fair, M. G., R. S. Gemmell, *J. Coll. Sci.19,* 360 (l964).

[45] Spicer, P.T., Pratsinis, S.E., Shear-induced flocculation: the evolution of floc structure and the shape of the distribution at steady state, *Water Research,* Elsevier Science Ltd., 30, (1996), pp.1049-1056.

[46] Pandya, J. D.; Spielman, L. A. Floc Breakage in Agitated Suspensions: Theory and Data Processing Strategy. J. Colloid Interface Sci. (1982), 90, 517.

[47] Boadway, J. D. Dynamics of Growth and Breakage of Alum Floc in Presence of Fluid Shear. J. Environ. Eng. Div. (Am. Soc. Civ. Eng.) (1978), 104, 901.

[48] Peng, S. J.; Williams, R. A. Direct Measurement of Floc Breakage in Flowing Suspensions. *J. Colloid Interface Sci.* (1994), 166, 321.

[49] Diemer, R. B., Olson, J. H., A moment methodology for coagulation and breakage problems: Part3 – generalized daughter distribution functions, *Chem. Eng. Sci*. 57 (2002) 4187 – 4198

[50] Kramer, T. A., Clark, M. M., Influence of strain-rate on coagulation kinetics, *Journal of Environment Engineering* ASCE 123 (1997), pp. 444–452

[51] P.J. Hill and K.M. Ng , New discretization procedure for the breakage equation. *A.I.Ch.E. Journal* 41 5 (1995), pp. 1204–1216

[52] Randolph, A. D., *A. I. Ch. E.J.* (1965), 11**,** 424.

[53] Konno, M., Matsunaga, Y., Arai K., Saito, S., Simulations model for break-up process in an agitated tank, *Journal of Chemical Engineering of Japan* **13** (1980), pp. 67–73

[54] Sathyagal, A.N., Ramkrishna, D. and Narsimhan, G., Solutions of inverse problems in population balances—II. Particle break-up. *Computers in Chemical Engineering* **19**, (1996) pp. 437–451

[55] Spicer, P. T., and Pratsinis, S. E. "Coagulation and Fragmentation: Universal Steady-State Particle-Size Distribution." AIChE J., 42(6), (1996a), 1612-1620.

[56] Smoluchowski M. V., Versuch einer mathematischen Theorie der Koagulationskinetik kolloider Lösungen, *Z. Phys. Chem.* **92,** (1917), 129-168

[57] Ramkrishna, D., The status of population balances (1985). *Rev. Chem. Eng.* **3,** 49-95.

[58] Song, M., Steiff, A. Weinspach, P. M., A very effective new method to solve the population balance equation with particle size growth, *Chem. Eng. Sci.*, Vol. 52, No. 20, (1997), pp. 3493-3498.

[59] Kapur, P.C., A Similarity solution to an integro-differential equation describing batch grinding. *Che, Eng. Sci*. **25**, 855-901.

[60] Ramabhadran, T. E., Seinfeld, J. H., Self preserving theory of particulate systems *Chem. Eng. Sci.*, 30, (1995), pp. 1019-1025.

[61] Das P. K., Ramkrishna D., Narsimhan G. Effect of mass transfer on droplet breakup in stirred liquid-liquid dispersions, *A. I. Ch. E.J.* **33,** (1987), 1899-1902

[62] Guilhem, X. D., Ring, T. A., Exact solution for the population in a continuous stirred tank crystallizer with agglomeration, *Chem. Eng. Sci.*, 42, (1987), pp. 1247-1249.

[63] McGrady E. D., Ziff, R. M., Analytical solutions to fragmentations with flow. *A. I. Ch. E.J.* **34,** (1988), 2073-2076.

[64] Lui R. Y., Thompson, R.W., Analysis of a continuous crystallizer with agglomeration (1992)

[65] Argyiou, D. T., List, H. L., Shinnar, R. Bubble growth by coalescence in gas fluidized beds. *A. I. Ch. E.J.* **17,** (1971), 122-130.

[66] Hashimoto K., Silveston, P. L., Gasification Part I. Isothermal, Kinetic control for model for a solid with a pore size distribution. *A. I. Ch. E.J.* **19,** (1973), 259-268.

[67] Kane, S.G., Evans, T. W., Brian, P. L. T., Sarofim, A. F., Determination of the kinetics of secondary nucleation in batch crystallizers. *A. I. Ch. E.J.* **20,** (1974), 855-862.

[68] Randolph, A. D., White, E. T., Modeling size dispersion in the prediction of crystal-size distribution. *Chem. Eng. Sci.*, 32, (1977), 1067-1076.

[69] Byrd, L. W., Mulligan, J. W., A population balance approach to direct-contact secondary refrigerant freezing. *A. I. Ch. E.J.* **32,** (1986), **1**881-1888.

[70] Singh, P. N., Ramkrishna. D., Solution of population balance equations by MWR. *Comput. Chem. Eng.* 1, (1977), 23-31.

[71] Bhatia, S. K., Chakraborty, D., Modified MWR approach: application to agglomerative precipitation. *A. I. Ch. E.J.* **32,** (1992), 868-878.

[72] Chen, M. Q., Hwang, C., Shih, Y. P. A Wavelet-Galerkin method for solving population balance equations. *Comput. Chem. Eng.* 1, (1996), 131-145.

[73] Frymier, P. D., Ford, R. M., Cunnings, P. T., Analysis of bacterial migration: I. Numercial solution of balance equation. *A. I. Ch. E.J.* **40,** (1994), 704-715.

[74] Nicmanis, M., Hounslow, M. J., A finite element analysis of the steady state population balance equation for particulate systems: aggregation and growth. *Comput. Chem. Eng.* **20**, (1996), S261-S266.

[75] Marchal, P., David, R., Klein, J. P., Villermaux J. Crystallization and precipitation engineering, I. An efficient method for solving population balance in crystallization with agglomeration. *Chem. Eng. Sci.*, **43**, (1988), 59-67.

[76] Kumar, J., Peglow M., Warnecke, G., Heinrich, S. The cell average technique for solving multi-dimensional aggregation population balance equations. *Comput. Chem. Eng.* **32**, (2008), 1810-1830.

[77] Viboolvorakul, W., Experimental investigation and mathematical modeling of a diffusion controlled disintegration process for TiO_2 nanoparticles, *Otto-von-Guericke Univ. Fac. Process and systems eng. M.Sc Thesis (2008).*

[78] Peltonen, L., Kainu, L., Hirvonen, J., Freeze-drying of poly(L-lactic acid) nanoparticles, *Journal of nanoscience and nanotechnology* 6(9-10): (2006), 3110-7.

[79] Schnettler, F.J., Monforte, F.R., Rhodes W.W. *Science of Ceramics*, (The British Ceramic Society, United Kingdom (1968).

[80] Johnson, D.W., Gallagher P.K.: *J. Am. Ceram.* Soc. Vol. 54 (1971), p. 440.

[81] Nieto M., Tallon, C., Moreno, R., Synthesis of Gamma-Alumina Nanoparticles by Freeze Drying, *Advances in Science and Technology Vol. 45 (2006) pp 223-230*

[82] Hintz, W., Nikolov, T., Tomas, J., Agglomeration and disintegration sub-processes occurring in the sol-gel precipitation of nanosized Titanium (IV)-oxide. Otto-von-Guericke Universität, Mechanical Process Engineering.

[83] Torrey DeLuca, Michael Kaszuba, and Kevin Mattison. Optimizing Silicone Emulsion Stability Using Zeta Potential, *American Laboratory News* June/July 2006.

[84] Gokhale, Y. P., Kumar, R., Kumar, J., Hintz, W., Warnecke, J., Tomas, J., Disintegration process of surface stabilized sol-gel TiO_2 nanoparticles by population balances. *Chem. Eng. Sci.* (2009).

[85] Hintz, W., Günther, T., Nikolov A., Petrova, A., Tomas, J. Production of nano-scaled silica, titania and barium sulphate particles – Experiments and modeling of particle formation micro-process. Dept of Process Engineering, Otto-von-Guericke Universität, Magdeburg, Germany.

[86] Ball, J.M., Carr, J., 1990. The discrete coagulation-fragmentation equations: existence, uniqueness, and density conservation. Journal of Statistical Physics 61, 203–234.

[87] Hintz, W., Ebenau, B., Tomas, J., Applied particle characterization methods for size, density, surface area and pore size. *Finite Particle Technology and characterization (2008)* 117 – 150.

[88] Moran, P. D.; Bartlett, J. R.; Bowmaker, G. A.; Woolfrey, J. L.; Cooney, R. P. *J. Sol-Gel Sci. Technol.*, **1999**, 15, 251.

Statement

To the best of my knowledge, this thesis work contains no material which has been presented for any other degree, or diploma at any other university. The scientific work contains no material that is published previously, communicated personally, or written by any other person except where the due reference is given.

I pledge myself to be the author who independently created all the work required for this thesis work.

November 30, 2009.

Olukayode Isaiah Imole

Otto-von-Guericke University, Magdeburg.